



**Analysis of roundness profiles of metal
cups after ironing with conventional and
adjustable punches**

Bachelor's Thesis

AUTHOR

Marta Pastor Robert - s230288

SUPERVISORS

Chris Valentin Nielsen
Kaarel Siimut

June 19, 2023

Abstract

When ironing stainless steel with a conventional, solid punch, the roundness achieved in the cups is quatrmodal (with big ears every 45°). However when deep drawn cups are ironed with the prototype of a new adjustable punch, designed by Kaarel Siimut in 2022, roundness of the cups turned to be bimodal. The goal of this project it to determinate why roundness turns bimodal when using the adjustable punch.

At the starting point of the project, it was discussed the different factors that could create this variation in the circular profile. The factors that are addressed in this project are:

1. Possible imperfections in the tools involved in the processes.
2. Influence of the deep drawing and ironing processes itself.
3. Influence of the materials of the cup, where stainless steel known as 1.4404 in European Standards (EN) and EN 1.4307 were analysed.

To study the first factor (possible imperfections in the tools involved in the processes), roundness of each of the tools was measured in Zeiss Coordinate Measure Machine (CMM). It was discover that no tool had any significant effect that would create this bimodal roundness.

The research then continued by analysing the influence of the deep drawing process by rotating the blank placed in the blankholder by 0° , 45° and 90° relative to a mark traced in the blankholder before a new deep drawing operation. The transformation of the blank to a cup commenced with a circular sheet of 61 mm diameter and 1 mm thick, with a sharp mark at the rolling direction. After deep drawing the cup, its roundness was measured using a scanning strategy with the CMM by recording the coordinates of 500 points at six circular profile at the cup walls: inner and outer surface at three different heights. It was found that after deep drawing roundness was quadratic regardless the material and the orientation set.

Later on, the same experiment was conducted but studying the ironing process. The ironing die was marked to set a reference to later rotate the cup. The 0 mark of the cup was rotated 0° , 45° , and 90° relative to the die's mark. Tools were kept in a constant position and orientation for each repetition, so that only the cup would rotate. Afterwards, roundness of the ironed cups was measured with CMM following the same procedure as deep drawn cups. It was found that for EN 1.4404 roundness

was bimodal, whereas for 1.4307 roundness did not follow any specific pattern. This led to think that bimodal roundness was caused by the reduction of the punch's stiffness when retracting the mandrel combined with a property of the material. Hence, the anisotropy of each material was studied through the tensile strength test in uniaxial load conditions to obtain the normal anisotropy (R-value) for each material. The tensile test specimens were cut forming 0° , 45° , and 90° relative to the rolling direction to obtain the normal anisotropy at each direction. The results showed that 1.4404 had a lower R_0 compared to the other directions, in addition to being more anisotropic than 1.4307.

This lower R_0 created a non-homogeneous thickness distribution after deep drawing at each section parallel to the flange plane. As the adjustable punch suffered a reduction of its stiffness when retracting the mandrel, it would then fit the thickness distribution of the plane at the end of the forward stroke, before the backstroke would be performed.

The final conclusion was summed up: the more anisotropic the material is, and the lower the R-value in one direction compared to the others, the higher the likelihood to obtain a bimodal roundness.

Keywords: deep drawing, ironing, roundness, EN 1.4404, AISI 316L, EN 1.4307, AISI 304L, thickness, anisotropy, R-value.

Preface

This thesis, of 15 ECTS, has been prepared over a period of 15 weeks between 6th March 2023 and 19th June 2023 in collaboration with the Department of Civil and Mechanical Engineering at the Technical University of Denmark (DTU) in partial fulfilment for the degree of Technology of Industrial Engineering Bachelor at the Polytechnical University of Valencia (UPV) during the Erasmus Program.

Signature:

A handwritten signature in black ink that reads "Marta". The script is cursive and elegant, with the 'M' being particularly large and stylized.

Acknowledgements

First, I would like to show my gratitude to [Chris Valentin Nielsen](#) who guided me during the project and whose knowledge was critical to discuss the final results, select the experiments and reach the final conclusions.

Thankful also with [Klaus Liltorp](#) who booked part of his time to teach me and explain, in various occasions, the use of the Zeiss Coordinate Measure Machine and its software.

Thank you to my family and my friends, specially my mom and dad, who supported me and helped me from their experience.

Finally, my most sincere gratitude to [Kaarel Siimut](#), who supported me during the entire project, guiding me in the experiments to conduct, helping in the brainstorming and discussion of the results, solving doubts, teaching how to use the machinery and equipment of the lab, contacting the necessary people to carry out the experiments, and always showed his help when needed. Sincerely grateful.

Nomenclature

Abbreviations

| | |
|------|--|
| AISI | American Iron and Steel Institute |
| CMM | Coordinate Measure Machine |
| DD | Deep Drawing |
| DIN | German Institute for Standardization |
| DTU | Technical University of Denmark |
| EN | European Standards |
| eq. | equation |
| I | Ironing |
| ISO | International Organization for Standardization |
| LSQ | Least Squares method |
| UPV | Polytechnical University of Valencia |

Physical variables

| | |
|------------|--|
| \bar{R} | Normal anisotropy weighted average |
| σ_r | Radial stress (Pa) |
| σ_t | Tangential stress (Pa) |
| σ_z | z stress (stress in the normal direction) (Pa) |
| t_0 | Thickness of the initial blank (m) |
| t_1 | Thickness after ironing (m) |
| t_{DD} | Thickness after deep drawing (m) |
| uD | Punch-die clearance (m) |

| | |
|------------------------|---|
| ΔL | Increase in length (m) |
| Δr | Planar anisotropy |
| Δw | Increase in width (m) |
| Δx | Increment in the spring length according to Hooke's Law (2.3) (m) |
| ϵ_{eq} | Equivalent strain |
| ϵ_l | Longitudinal strain |
| ϵ_t | Thickness strain |
| ϵ_w | Width strain |
| ϵ | Strain |
| σ | True stress (Pa) |
| σ_N | Nominal or engineering stress (Pa) |
| F_{BH} | Blankholder Force (N) |
| F_{measured} | Force measured by the press during ironing (N) |
| F_{real} | Real force applied to the deep drawn cup during ironing (N) |
| F_{springs} | Force of the springs in the subpress (N) |
| p_{BH} | Blankholder pressure (Pa) |
| T | Torque applied to the mandrel (N m) |
| LDR | Limiting draw ratio (m) |
| R | R-value |
| R-value | Normal anisotropy |

Contents

| | |
|---|------------|
| Abstract | i |
| Preface | iii |
| Acknowledgements | v |
| Contents | ix |
| 1 Introduction | 1 |
| 1.1 Motivation | 1 |
| 1.2 Relation with the subjects studied | 1 |
| 1.3 Materials | 2 |
| 1.4 Deep drawing axisymmetric cups | 2 |
| 1.4.1 Anisotropy in deep drawing | 5 |
| 1.5 Ironing | 5 |
| 1.5.1 Ironing with the adjustable punch | 6 |
| 1.6 Discussion of Siimut's results | 9 |
| 1.6.1 Deep drawing results | 9 |
| 1.6.2 Ironing results | 11 |
| 1.7 Conclusions after Siimut's results | 14 |
| 2 Experimental Procedure | 19 |
| 2.1 Manufacturing process of the cups | 19 |
| 2.2 CMM measurements | 19 |
| 2.2.1 Tools | 20 |
| 2.2.2 Cups | 22 |
| 2.3 Deep drawing | 25 |
| 2.4 Ironing | 29 |
| 2.5 Tensile strength test procedure | 32 |
| 3 Material Properties: Anisotropy | 35 |
| 3.1 True stress-strain curve | 35 |
| 3.2 R-value | 37 |

| | | |
|----------|---|-----------|
| 4 | Results and Discussion | 39 |
| 4.1 | CMM measurements of the tools | 39 |
| 4.1.1 | Deep drawing die | 39 |
| 4.1.2 | Deep drawing punch | 40 |
| 4.1.3 | Ironing mandrel (adjustable punch) | 40 |
| 4.1.4 | Ironing die | 42 |
| 4.1.5 | Ironing punch | 42 |
| 4.1.6 | Conclusion | 43 |
| 4.2 | Deep drawing: roundness | 43 |
| 4.2.1 | 1.4404 | 44 |
| 4.2.2 | 1.4307 | 45 |
| 4.3 | Ironing | 47 |
| 4.3.1 | Ironing punch force | 47 |
| 4.3.2 | Roundness | 48 |
| 4.3.2.1 | 1.4404 | 48 |
| 4.3.2.2 | 1.4307 | 49 |
| 4.3.3 | Discussion | 50 |
| 5 | Conclusions and Further Research | 53 |
| | Bibliography | 55 |
| | Appendices | 57 |
| | Python Scripts | 59 |
| | Roundness of the cups | 59 |
| | Thickness distribution of the cups | 61 |
| | Springs of the subpress | 62 |
| | Ironing punch force | 64 |
| | Tensile strength test | 65 |
| | Additional CMM Measurement of the Cups | 67 |
| | Deep drawing | 67 |
| | 1.4404 | 67 |
| | 1.4307 | 70 |
| | Ironing | 70 |
| | 1.4404 | 70 |
| | 1.4307 | 71 |
| | Calibration Certificates | 80 |
| | Axial extensometer | 80 |
| | Transverse extensometer | 82 |
| | Demonstrations | 83 |

| | |
|---|-----------|
| Equivalent strain in plane stress | 83 |
| Sustainable Development Goals | 85 |

CHAPTER 1

Introduction

1.1 Motivation

This thesis dates back to the Master's Thesis developed by Kaarel Siimut in 2022 [1], where bimodal roundness achieved after ironing cups with the adjustable punch did not have an explanation and needed to be studied in more detail. In said thesis, Siimut developed a new punch for cups ironing, which reduced its stiffness after the forming stroke and consequently its diameter was reduced by a few micrometers, minimizing the work done during the backstroke. Hereinafter the punch designed will be known as adjustable punch. From the design of said adjustable punch, the roundness of the inner circular profiles of the cups was measured with CMM Zeiss (Coordinate Measurement Machine). It was observed that unlike ironing with a conventional punch, where the roundness tended to be four-modal, using the adjustable punch the roundness was bimodal (similar to an ellipse). This is why, it was decided to open an additional line of research that studied carefully the effects of ironing with the adjustable punch. Thus, the main objective of this Bachelor's Thesis is to determine the factors that contribute to create a bimodal roundness when ironing with the adjustable punch.

1.2 Relation with the subjects studied

Polytechnical University of Valencia

- "*Materials Science*", code 11411, 3rd semester.
- "*Materials Technology*" code 11422, 6th semester.
- "*Production and Manufacturing Systems*", code 11416, 5th semester.

Technical Univerisy of Denmark (DTU)

- "*Introduction to Programming and Data Analysis: Python*", code 02631, 8th semester.

For the development of the thesis, the student learned to use the drawing and ironing machines of the DTU laboratory, and the Coordinate Measurement Machine (CMM) and its software, to program the measurement plan and base alignment. At the same time, the student developed a deep knowledge of Python to process and plot the data, since 500 points of 6 circumferences per cup were measured for 3 repetitions per material and orientation, for 3 orientations, for 2 materials, for 2 processes, representing a total of 216 files with the Cartesian coordinates of these 500 points each. In this way, Python was necessary to be able to analyse the results and draw conclusions.

1.3 Materials

The materials used for this project are two different alloys of stainless steel.

The first alloy is EN 1.4404, equivalent to 316L in the American Iron and Steel Institute (AISI). Stainless steel 1.4404 has a wide range of applications, such as construction encasement, offshore modules, warehousing and overland transportation of chemicals, food and beverages, pharmacy... [2]. Its chemical composition in percent of the elements presented in the alloy is collected in Table 1.1.

| C | Cr | Mn | Si | P | S | Ni | N | Mo |
|------|-------------|------|------|-------|-------|-------------|------|-------------|
| 0.03 | 16.50-18.50 | 2.00 | 1.00 | 0.045 | 0.015 | 10.00-13.00 | 0.10 | 2.00 – 2.50 |

Table 1.1. Chemical composition of stainless steel EN 1.4404 in percentage presented [2]

The second material is known as EN 1.4307 or AISI 304L, used the industry for springs, screws, nuts and bolts, architectural panelling, tubing, brewery, food, dairy and pharmaceutical production equipment, sanitary ware and troughs, and cutlery and flatware, among others [3]. Chemical composition in percentage of the elements presented in the alloy:

| C | Cr | Mn | Si | P | S | Ni | N | Fe |
|------|-------------|------|------|-------|-------|------------|------|---------|
| 0.03 | 17.50-19.50 | 2.00 | 1.00 | 0.045 | 0.015 | 8.00-10.50 | 0.10 | Balance |

Table 1.2. Chemical composition of stainless steel EN 1.4307 in percentage presented [3].

1.4 Deep drawing axisymmetric cups

Deep drawing is one of the most popular metal forming processes used in different industries such as automotive, aerospace or packaging. Cylindrical cups are achieved by radially drawing a metal blank into the die circular cavity. As the punch deep

draws the metal blank into the die, the blank adjusts through plastic deformation the shape of the cylindrical punch [4].

The case of studio is deep drawing axisymmetric cups, starting with a round blank of 61 mm diameter and 1 mm thickness. Figure 1.1 represents a sketch of the process. As the punch moves through the die, the sheet starts to deform, until the desired stroke is achieved, which must be properly calculated to avoid fractures. Then the punch moves backwards to its original position. The ideal deep drawing process achieves a constant thickness distribution in all the points contained in the same plane parallel to the flange plane, although thinner thickness at the bottom and wider at the top is achieved.

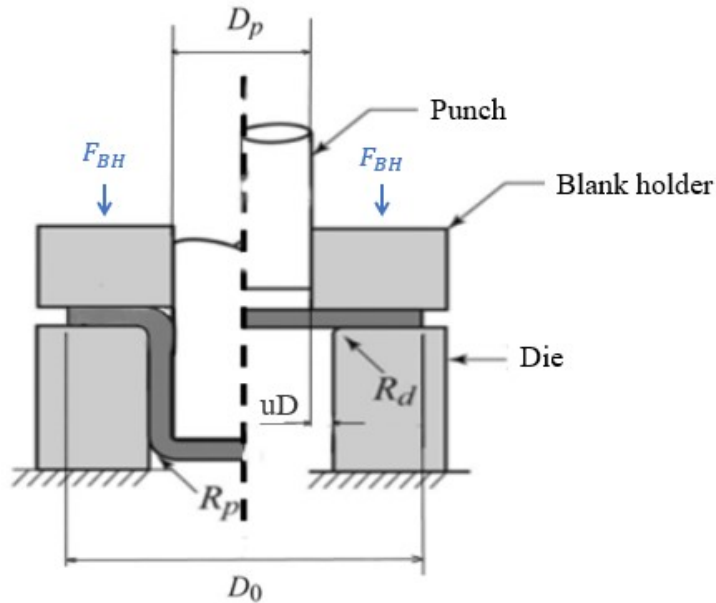


Figure 1.1. Deep drawing of axisymmetric cups. Modification from [5].

The punch-die clearance, uD is a parameter that depends on the initial blank thickness t_0 . This parameter is important to later select the deep drawing tools so that they will fit the blank thickness. For stainless steel, the recommended punch-die clearance is obtained with Equation 1.1 [6, p.111].

$$uD = t_0(1 + 0.07\sqrt{10}) \quad (1.1)$$

So that the process occurs successfully, there are several parameters to consider, being the most important the materials of the tools, the speed of the punch, friction and the blankholder force.

Blank holder force (F_{BH})

The blank holder force is the most important easily controllable parameter for achieving large cup heights [1, p.12,13]. This certain force can be obtained by multiplying the blankholder pressure required by the area. The blankholder pressure is defined by an empirical expression:

$$p_{bh} = 0.001c \cdot [(DR - 1)^3 + 0.005 \cdot \frac{d_o}{t_o}] \cdot S_u \quad (1.2)$$

where c is an empirical factor, usually between 2 and 3, d_o (mm) is the initial blank diameter, DR is the draw ratio defined as d_o/d_p and S_u (MPa) is the ultimate tensile strength of the material [6, p.107-112].

The draw ratio (DR) defines the final cup height, but it is limited to the maximum value that the cup can deform without fracture. This maximum value is named limiting draw ratio (LDR) and can be increased by reducing the blankholder force or increasing the punch or die corner radius [6, p.108]. The final walls of deep drawn cups are not cylindrical but conical, and thinner near the bottom.

Stress conditions

During the deep drawing process, different stress conditions result in the material which later conducts to strain forming. Figure 1.2 shows a drawn cup with the different loading zones: the flange, the cup wall, and the bottom. In the flange area, the radial direction suffers a tensile load, whereas compression load is found in the tangential direction [7].

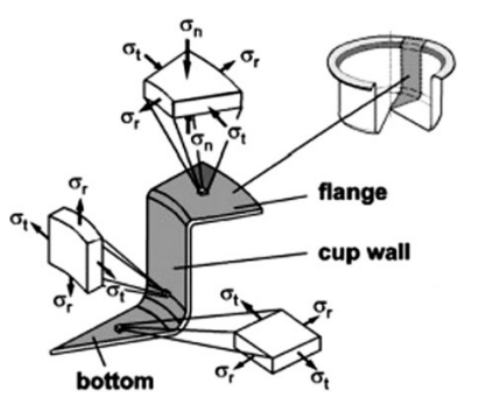


Figure 1.2. Stress-conditions in a drawn cup [7].

where σ_r refers to the radial stress, σ_t , tangential stress, and σ_n to the normal stress, that in this thesis will be known as z stress (σ_z).

1.4.1 Anisotropy in deep drawing

During deep drawing, there is a relationship between the material flow in the flange plane and the sheet thickness. This behavior is described by the normal anisotropy R , which is estimated via the tensile strength test under uniaxial load conditions. "The R -value is the ratio of the true plastic width strain to the true plastic thickness strain in a metal specimen that has been subjected to uniaxial tensile stress" [8].

$$R_\alpha = \frac{\epsilon_w}{\epsilon_t}, \quad (1.3)$$

where α is the relative angle to the rolling direction: 0° , 45° , and 90° .

The ability of the material to flow within the sheet plane increases with higher normal anisotropy. Therefore, a higher R -value corresponds to a better deep drawability. R -values of approximately $R=1$ means that the material is more isotropic and its flow will occur equally within the sheet plane as well as from the thickness [7], whereas $R>1$ means a larger resistance to thickness reduction [9]. Furthermore, the normal anisotropy R may vary in each direction of the sheet. A characteristic value to define this variation of R in the direction is the planar anisotropy Δr , [7].

$$\Delta r = \frac{R_0 + R_{90} - 2R_{45}}{2} \quad (1.4)$$

The closer to zero this value is, the more that it indicates equal metal flow in all directions, eliminating the ears forming. On the contrary, when $\Delta r \neq 0$.

Another meaningful parameter to study the variation of R in different directions in the plane of the sheet is the normal anisotropy \bar{R} , a weighted average of the R -values at each direction [9].

$$\bar{R} = \frac{R_0 + 2R_{45} + R_{90}}{4} \quad (1.5)$$

1.5 Ironing

The thickness distribution along the walls of a deep drawing cup is not homogeneous, but the upper two-thirds of the cup wall are thicker than the original blank. For this reason, deep drawn cups suffer a secondary metal forming process were walls are lengthen and uniform thickness is achieved, although thicker wall section is left in the curvature near the bottom. If a deep drawn cup is redrawn, the thickness at the top may be up to 50% of the original thickness. Therefore, an ironing operation is needed to produce uniform wall thickness [10]. Ironing also reduces the residual stresses present in the cup walls after deep drawing [6, p.416]. The total thickness reduction (TR) from a flat blank to an ironed cup is defined as:

$$TR = 1 - t_1/t_0, \quad (1.6)$$

where t_1 is the cup wall thickness after ironing and t_0 is the nominal blank thickness before deep drawing [1, p.4].

The ironing operation may be performed either on the inside or the outside surface of the deep drawn cup, both leading to an increase in cup height since the volume of the blank remains constant during the process. In inner ironing the punch is the forming tool, and the die is the supporting tool [11, p. 125, 127]. As the innovative adjustable punch was designed to iron the inner surface, ironing was performed from the inside. In Figure 1.3 a sketch of the ironing process is pictured, where t_{DD} represents the thickness of the deep drawn cup and t_1 is the thickness after ironing.

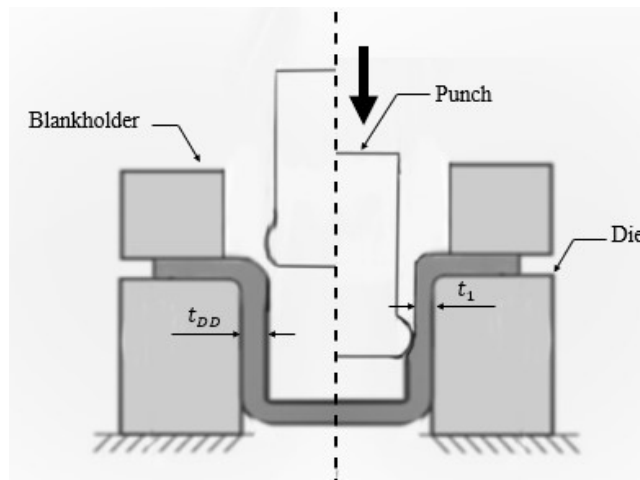


Figure 1.3. Ironing from the inside.

When ironing the inner surface a blankholder and a flange are required. Inner ironing includes a backstroke, where the punch is still in contact with the blank what creates high contact pressures although the blank is barely deformed. The punch stroke is limited by the cup bottom [1, p.4, 5].

Low friction in the contact surfaces between the punch and the blank is desired, whereas high friction between the die and the blank is wished to increase the thickness reduction. For this reason, the supporting tool (the die) is often slightly roughened [11, p.125].

1.5.1 Ironing with the adjustable punch

When ironing, the uniform thickness distribution is achieved in the forward stroke, where a compressive punch force is necessary. Hence, the work done during retraction is superfluous. However, when the punch is retracted, tensile punch force is generated due to friction and elastic spring-back of the ironed cup and the ironing tools, which is often around 50% of the ironing force. The aim of the design of the adjustable

punch is to minimize the backstroke work. This could be achieved by reducing the diameter of the ironing punch when it reaches the bottom dead center (at the end of the ironing stroke) [10]. Or, in other words, increasing the punch diameter before the forming stroke by inserting the mandrel, and reducing it to its relaxed dimensions before the backstroke extracting the mandrel.

The ironing experiments conducted in this thesis used the prototype of this innovative punch, hereby described according to [10]:

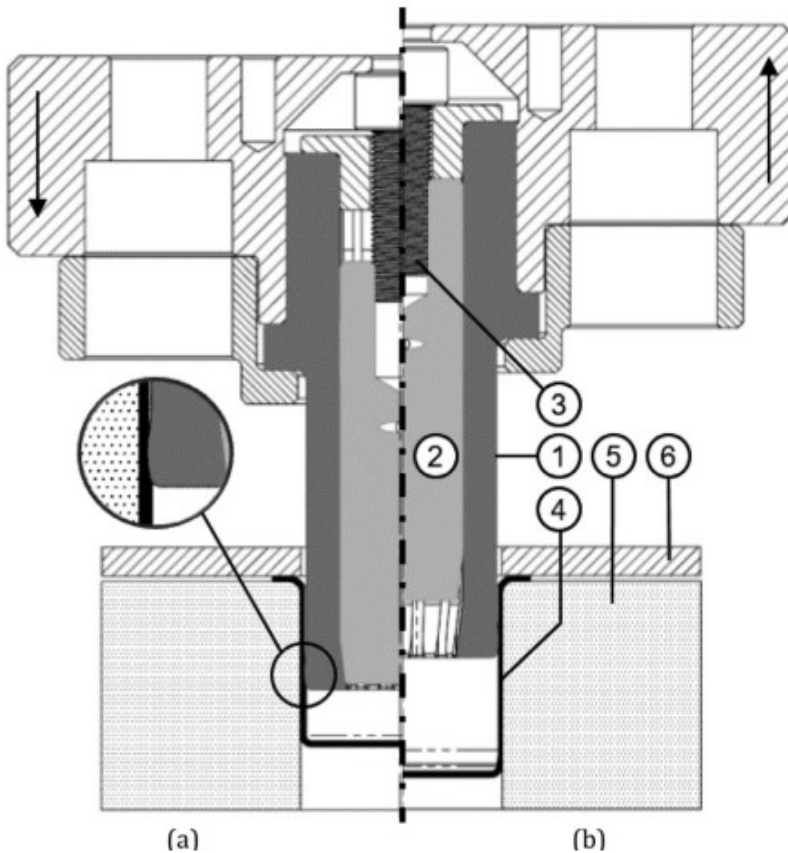


Figure 1.4. Sectional view of prototype ironing punch with adjustable diameter shown during (a) ironing and (b) retraction. The main components are (1) hollow punch, (2) mandrel, (3) actuator screw, (4) workpiece, (5) die, and (6) blank holder for clamping the workpiece flange. Figure obtained from [10].

”The core of the tool is that the conventional solid punch is replaced by a hollow punch sleeve (1) with an internal mandrel (2), which can be axially positioned by a grade 12.9 fine-threaded $M10 \times 1.0$ screw (ISO 12474) (3). The punch diameter

of the prototype was $\varnothing 33.8$ mm, and the diameter of the mandrel was $\varnothing 21.2$ mm. When ironing (Figure 1.4 a), the mandrel is inserted to support the punch sleeve reproducing a conventional, solid punch. During retraction, the mandrel is extracted to the position shown in Figure 1.4 what reduces the radial punch stiffness, that leads to a decrease in the contact pressure between the punch and the ironed cup (4).”

”12 slits are revealed along the inside of the punch sleeve. The slits are 2.1 mm wide and leave 2.4 mm from the slits to the widest point on the punch nose. These slits were included in the prototype design for a compromise between resistance towards buckling and reduced circumferential stiffness, and for showcasing space for lubrication channels” [10].

The interface between the mandrel and the punch sleeve when the mandrel is inserted was designed conical, with a semicone angle of 7° , given that the conical interface makes it possible to increase the punch diameter when inserting the mandrel. A bottom view of the punch and the mandrel is pictured in Figure 1.5, with the mandrel inserted (Figure 1.5 a) and the mandrel retracted (Figure 1.5 b) [10].

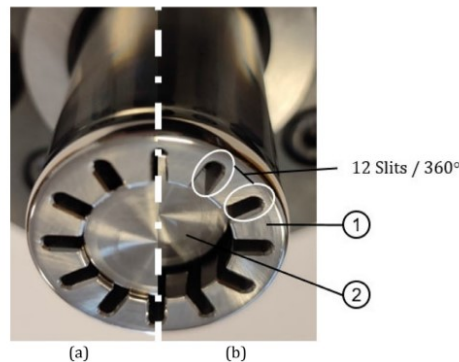


Figure 1.5. Photographs of the adjustable punch showing (1) the hollow punch including 12 slits and (2) the mandrel in axial position corresponding to (a) ironing and (b) retraction. Figure obtained from [10].

The punch sleeve is made of Vanadis 4 Extra SuperClean with a hardness of 62 HRC. The mandrel is made of Sleipner hardened to 63 HRC. The prototype tool presented here is uncoated [10, p.2]. No sign of the 12 slits were found on the ironed cups in the measured roundness profiles [10, p.3].

The results obtained after analysing the axial force during the forward and back-stroke of ironing with a conventional punch and with the adjustable punch prototype are shown in Figure 1.6, where new punch refers to the new adjustable punch designed, and T (N m) is the torque applied to insert the mandrel.

The axial forces measured during ironing (compressive forces) were similar for all cases, while the axial force during retraction (tensile) was reduced almost halved when the mandrel was retracted before extraction. The tightening torque T was found to

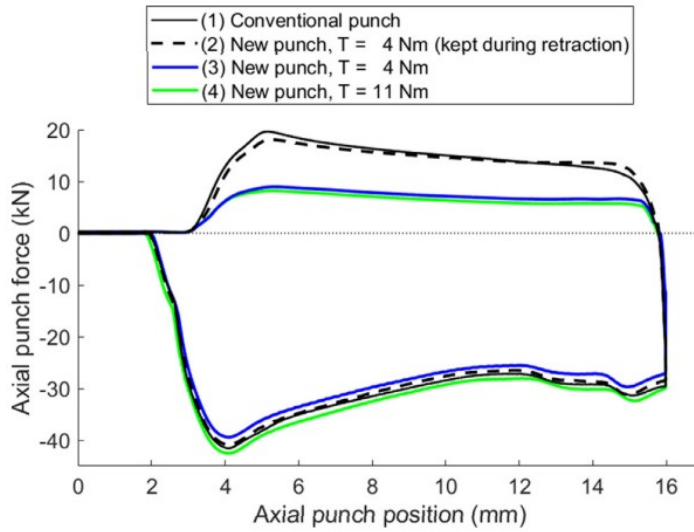


Figure 1.6. Measured force-position curves during ironing and retraction for the four punch configurations, obtained from [10].

have a small influence. When $T = 11 \text{ N m}$, the diameter was greater than that of the conventional punch resulting in an increased ironing force. On the contrary, when $T = 4 \text{ N m}$, the punch diameter and the ironing force were smaller [10, p.3, 4].

1.6 Discussion of Siimut's results

The results that Kaarel Siimut obtained during his Master's Thesis are analysed in the following lines.

1.6.1 Deep drawing results

In page 105 of Siimut's Thesis [1] the results of the roundness measured with CMM after deep drawing **laser cut EN 1.4307** blanks can be found. The stroke length was set to 17.7 mm for all cups, and the lubricant he used was Rhenus SU 500A.

From the Figures 1.7 and 1.8 it is observed that a quadratic roundness appeared, easier to visualize in the inner diameter when applying 6.33 kN force to the blankholder.

Keeping the material constant and the cutting method, and just varying the F_{BH} , in both cases a quadratic model appears, but the lower the F_{BH} applied the best to distinguish a quadratic shape.

Other aspect to consider was that the noticeable maximums of the quadratic model always appears at the same location, approximately every 45 degrees.

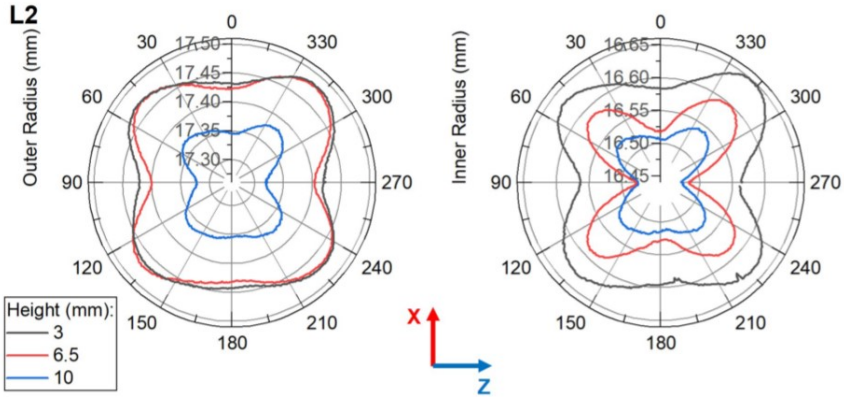


Figure 1.7. Roundness of outer (left) and inner (right) diameter at three heights after deep drawing, applying a blankholder force of 6.33 kN [1, p.105].

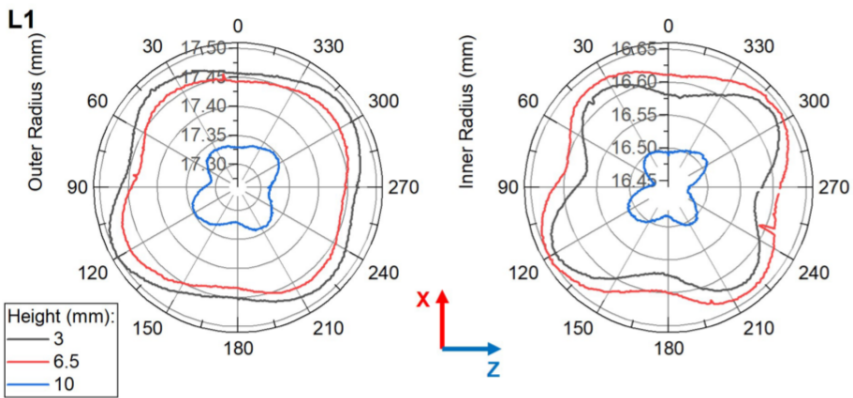


Figure 1.8. Roundness of inner (right) and outer (left) diameter at three heights after deep drawing, applying a blankholder force of 10.55 kN [1, p.105].

1.6.2 Ironing results

Below are shown the measurements of roundness of the inner (right) and outer (left) diameter measured at three different highs (3, 6.5 and 10 mm) after ironing 18 deep drawn cups that came from deep drawing **sheared EN 1.4404** blanks using a blankholder force of 10.55 kN, a deep drawing stroke length constant of 17.7 mm, and later a constant ironing stroke length of 16 mm.

Conventional punch:

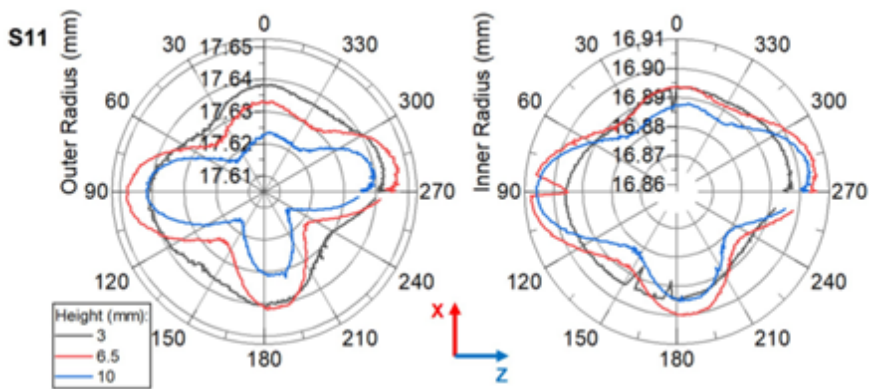


Figure 1.9. Conventional punch: inner (right) and outer (left) diameter of ironed cup [1, p.122].

In addition, ironing with the adjustable punch with the mandrel inside during retraction (adjustable punch working as conventional), roundness was also quadratic:

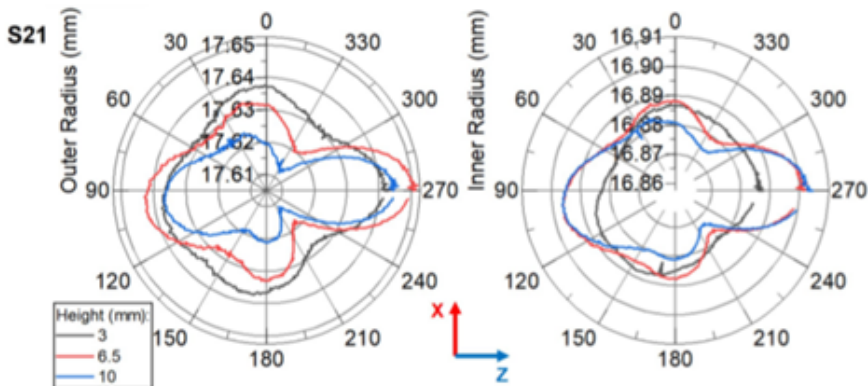


Figure 1.10. Adjustable punch as conventional: inner (right) and outer (left) diameter [1, p.122].

For both ironing processes it was observed that the cup maintained the quadratic roundness, as it occurred in the previous section after deep drawing (section 1.6.1).

Nevertheless, the results obtained after ironing with an adjustable punch were different from the results previously presented.

Adjustable punch with the mandrel retracted

A) Uncoated punch and mandrel:

A.1) Torque = 4 Nm

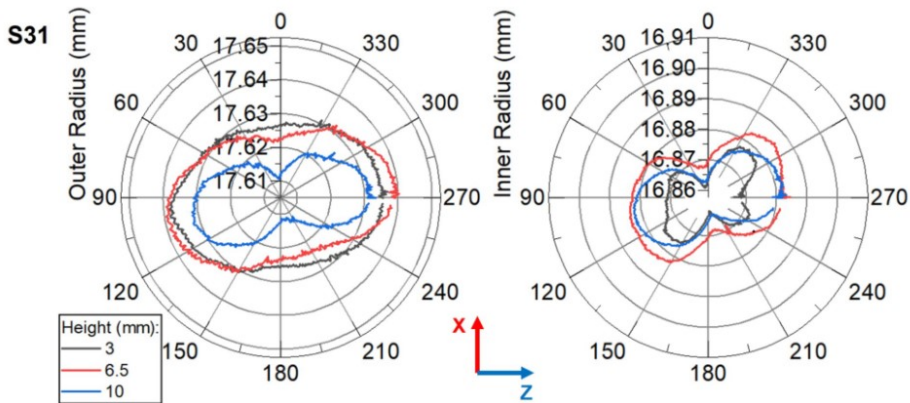


Figure 1.11. Adjustable punch: roundness of inner and outer diameter, punch and mandrel uncoated, $T=4$ Nm [6, p.123].

A.2) Torque = 11 Nm

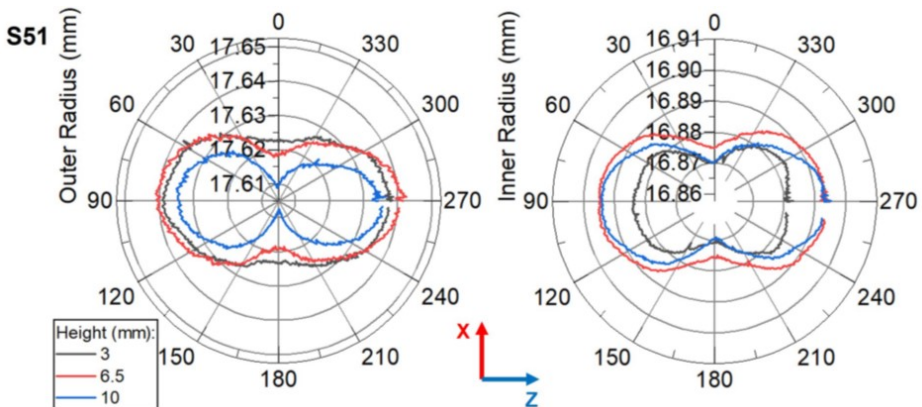


Figure 1.12. Adjustable punch: roundness of inner and outer diameter, punch and mandrel uncoated, $T=11$ Nm [6, p.123].

- B) Coated punch and mandrel:
 B.1) $T=4$ Nm

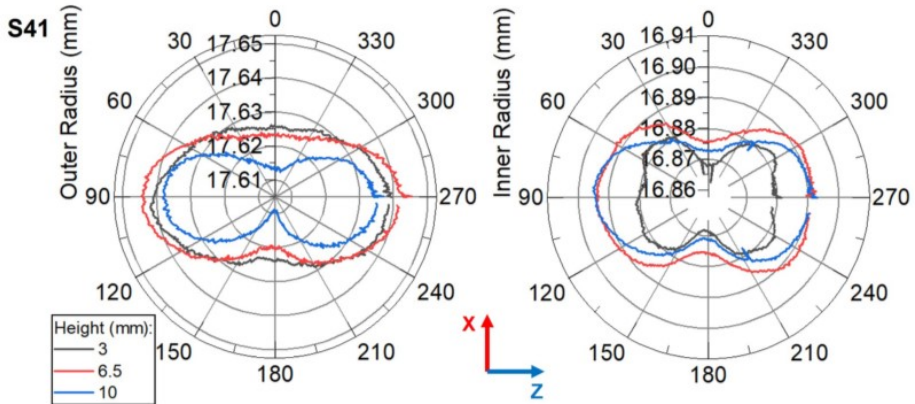


Figure 1.13. Adjustable punch: roundness of inner and outer diameter, punch and mandrel coated, $T=4$ Nm [6, p.124].

- B.2) $T= 11$ Nm

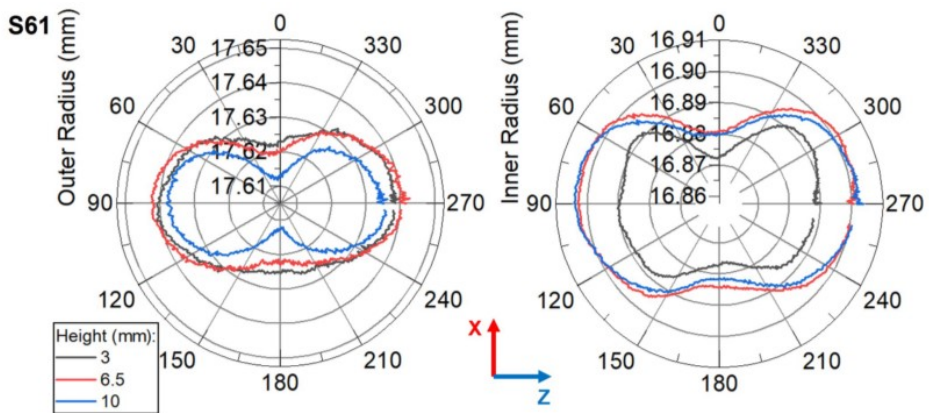


Figure 1.14. Adjustable punch: roundness of inner and outer diameter, punch and mandrel coated, $T=4$ Nm [6, p.124].

The use of coated or uncoated tools had no significant influence. In addition, it was observed that roundness after ironing with an adjustable punch was likely to be elliptical, independently of the material of the punch and the mandrel, or the torque applied.

1.7 Conclusions after Siimut's results

From previous section it was concluded that roundness after deep drawing was quadratic and it conserved that tendency after ironing with a conventional punch -or an adjustable punch maintaining the mandrel before retraction. However, when 1.4404 cups were ironed with the adjustable punch retracting the mandrel before the back-stroke, roundness turned into an elliptical shape.

The mind map bellow gathers a brainstorming of the possible factors that may cause this elliptical roundness.

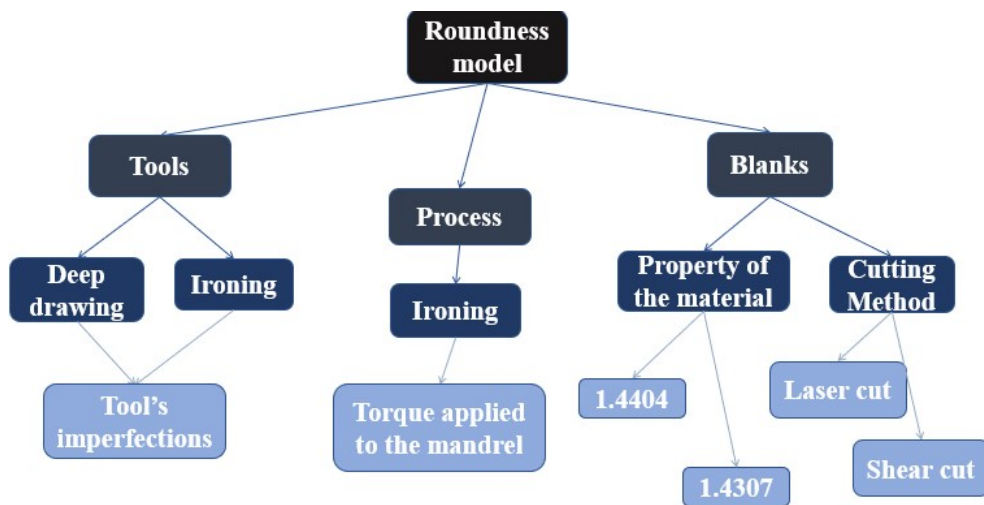


Figure 1.15. Mind map of the factors that may affect the roundness model.

In this way, the following experiments were designed to study each of the factors above mentioned:

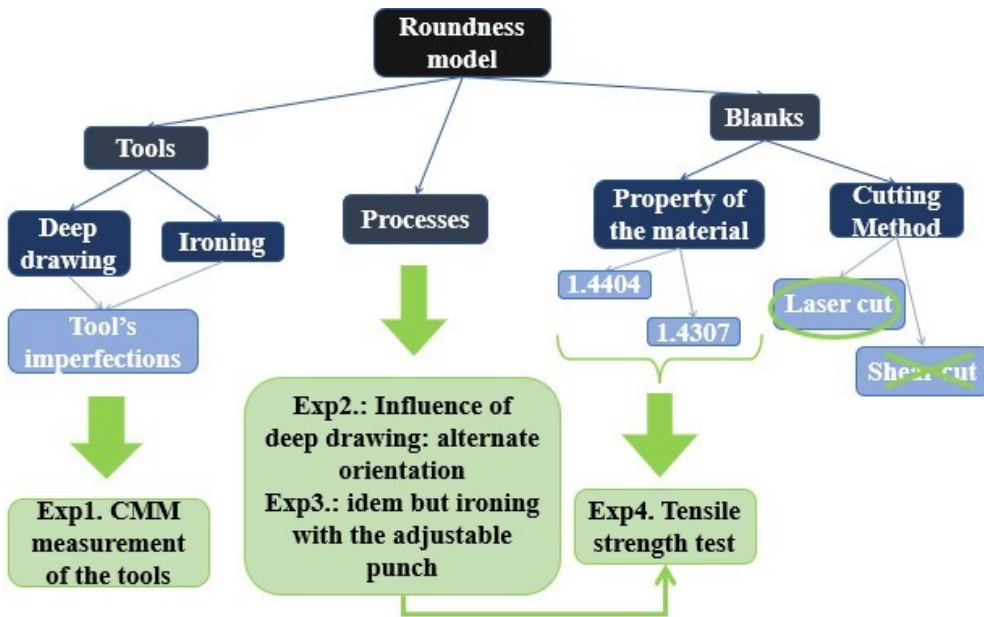


Figure 1.16. Mind map of the experiments to study each factor that may affect the roundness model.

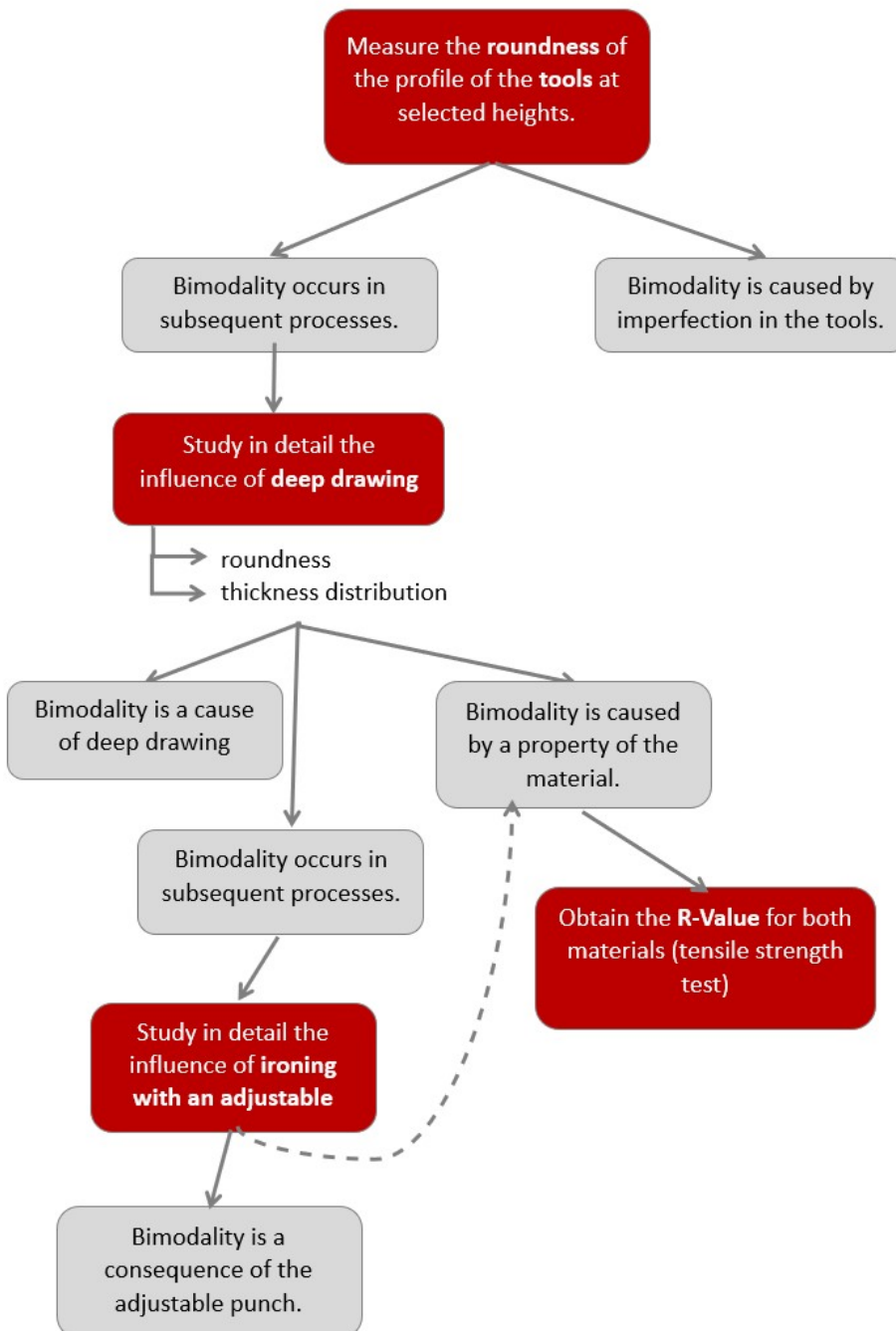


Figure 1.17. Chart flow of the experiments conducted.

CHAPTER 2

Experimental Procedure

2.1 Manufacturing process of the cups

Independently of the material used, the cups started from a laser cut flat blank of 61 mm diameter and 1 mm thickness (thickness of the sheet provided by the manufacturer).

The initial blank suffered two processes to become a finished cup. The first process consisted in deep drawing the initial blank to achieve the form of the cup. Secondly, the deep drawn cup was ironed so that the walls of the cup become thinner and taller, with a more homogeneous thickness distribution.

2.2 CMM measurements

In order to remove the uncertainty caused by the tools, their diameter and roundness was measured at a strategic heights using Zeiss DuraMax Coordinate Measuring Machine (CMM). Hence, it was measured:

1. Deep drawing die.
2. Deep drawing punch.
3. Ironing mandrel.
4. Ironing die.
5. Ironing punch.
6. Deep drawn cups.
7. Ironed cups.

For each of the circular profile a scanning strategy programmed recorded the Cartesian coordinates of 500 points at a speed of 90 mm/s, which were saved in a

text file. Later, these text files were processed and useful plots were represented using the Python script programmed (view in Appendix 5). The measurement program was prepared using Zeiss CALYPSO 2021 software. Least squares diameters of each circle were computed together with roundness of inner and outer diameters measured at the same plane.

2.2.1 Tools

CMM counts with different shaped stylus which are selected depending on the surface of the piece that needs to be accessed to accomplish the measurements. To perform the measurement of the tools, a ruby straight stylus was selected because of its simplicity in use and in programming. Tools were properly fixed using the equipment required.

As all the tools to be measured were axisymmetric, the bases alignment set for each were very similar. To define the x, y and z origin, the interception point between the top plane and the axisymmetric axis was chosen, and the planar rotation was defined with a line contained in the mentioned top plane, in the x-axis direction. As they were axisymmetric, there was no need to define the spatial rotation. Both, the top plane and the x-axis of each tool are defined in the following lines, in addition to the heights selected to measure each tool. For all of them, the x, y and z origin is shown in the figures as the center where the three axis (blue, green and red) intercept.

The 3D prototypes of the tools and the cup contained in Figures 2.2, 2.3, 2.4, 2.5 and 2.6 were made by Kaarel Siimut for his Master's Thesis [1].

Deep drawing die

The inner diameter of the deep drawing die was measured at -2.5 and -5.5 mm from the top plane (pink in Figure 2.1) in the z direction (blue in Figure 2.1).

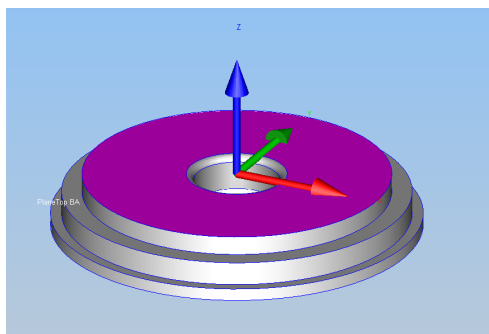


Figure 2.1. Deep drawing die top plane (pink), x-axis (red), z-axis (blue) and coordinates origin.

Deep drawing punch

The heights selected to measure the deep drawing punch were -2.5, -6 and -11 mm from the top plane (pink in Figure 2.2) in the z direction (blue in Figure 2.2).

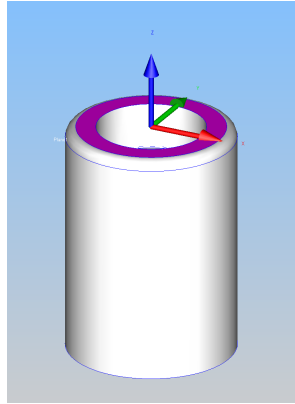


Figure 2.2. Deep drawing punch top plane (pink), x-axis (red), z-axis (blue) and coordinates origin.

Ironing mandrel

It was chosen to measure the diameter and roundness at -0.5, -2.5, -4.5 and -6.5 mm in the z-axis from the top plane (pink in Figure 2.3).

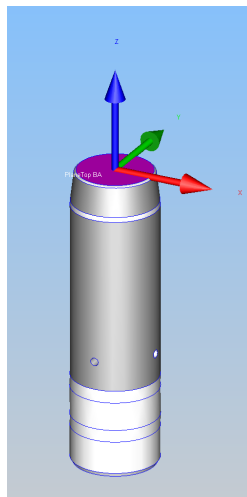


Figure 2.3. Ironing mandrel top plane (pink), x-axis (red), z-axis (blue) and coordinates origin.

Ironing die

Furthermore, the ironing die was measured at -3, -6.5 and -10 mm.

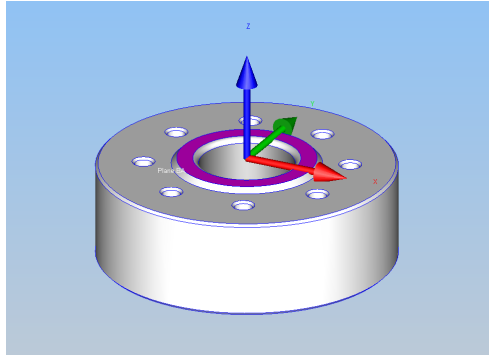


Figure 2.4. Ironing die top plane (pink), x-axis (red), z-axis (blue) and coordinates origin.

Ironing punch

Finally, the ironing punch was measured at the maximum of its torus. Being this maximum at -3.122 mm from the top plane in the z direction.

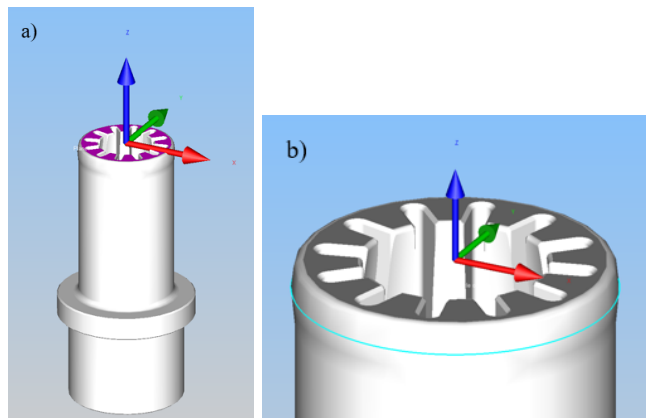


Figure 2.5. a) Ironing punch top plane (pink), x-axis (red), z-axis (blue) and coordinates origin, b) circular profile at the maximum of the torus (light blue).

2.2.2 Cups

For both, deep drawn and ironed cups, the diameter and roundness of the walls were measured at three different heights both on the inner and outer surface. The measurements were performed with a four-way star stylus using two of the styli (No 2

and No 4) with 5 mm spherical tip and 32 mm shaft lengths. The probing system was qualified with the master probe each new day that measurements were performed.

The cup was placed vertically, meaning that the axisymmetric axis is parallel to the floor plane. Every cup measured was placed with the same orientation, placing the 0 mark at the top. The Python script was later programmed so that the plots always showed the 0° at the top, corresponding to the 0 mark of the cup (the rolling direction). The heights selected to measure the inner and outer diameter of the deep drawn and the ironed cups were 4, 6.5 and 10 mm from the flat base plane (view in Figure 2.6). Heights lower than 4 mm were not possible to access since the own radius of the stylus prevented the pass.

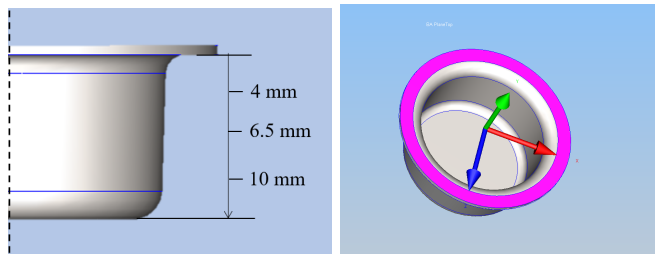


Figure 2.6. Sketch of the heights selected to measure the cups roundness (left), and reference axis (right): x-axis (red), y-axis (green), and z-axis (blue).

The cups were held from the opposite extreme at the 0 mark. In this way, the holder blocked the pass of the stylus for the outer circumferences in depths lower than 8 mm. For this reason, 4 and 6.5 mm heights missing points recorded are found from 135° to 225° at the outer diameter.

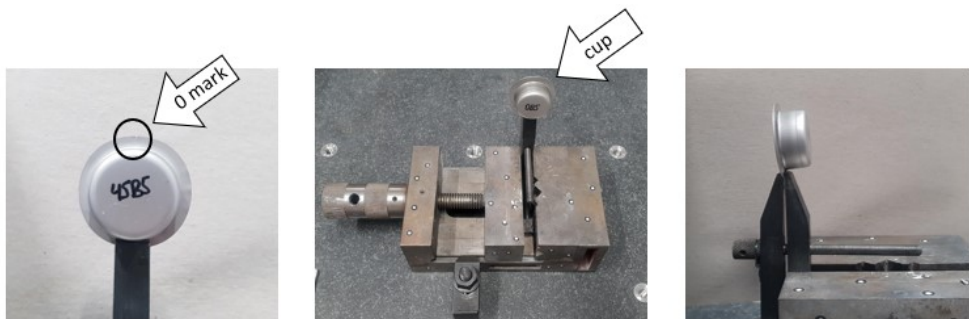


Figure 2.7. Cup holding for CMM

Base alignment (Figure 2.8) was established using eight points of the bottom surface (yellow), eight points on the surface of the flange (blue) and two circles (20 points each) at the outer surface of the walls of the cup (red).



Figure 2.8. Cup with surfaces used for establishing base alignment. Blue: top plane of the flange, yellow: bottom plane, and red: outer walls surfaces.

The recorded data points were exported in Cartesian coordinates and processed using again a Python script. This script fitted in two dimensions the data points to a least squares circle using an algorithm adapted from [12]. The 2D point cluster was subsequently transformed to polar coordinates and plotted. As points are 3-Dimensional, before fitting them to the least squares circle it was assured that the points were enclosed in the same plane. Technically, CMM strategy was programmed to accomplish it. However, it was checked that the angle formed between the farthest y coordinate and the XZ plane at that height compared with the radius of the wall cup at that specific height (r) was below 0.05° .

$$\theta = \text{atan}\left(\frac{y_{\max}}{r}\right) < 0.05^\circ \quad (2.1)$$

It was checked that the angle was incredibly small, in the range of 0.015° , and it could be assumed that y coordinate was negligible, and x and z coordinate could be assumed to be all contained in the same plane.

The manual base alignment was made for the first cup. The next cups to be measured were placed in the same position, but of course when placing them there was a deviation between the center of the cup of the base alignment $(0,0,0)$ and the center of the next cup placed. This center deviation caused that the reference system of the coordinates of the collected points was not the interception point between the top plane and the axisymmetric axis of the cup, which subsequently slightly displaced the plots represented. To solve this displacement, the Python script calculated the center of the closest circle fit using the modification from [12] and translated to $(0,0)$.

The plots were compared with the plots provided by the Zeiss CALYPSO software to verify that the roundness distribution was alike and no mathematical error had been committed when programming the script.

2.3 Deep drawing

To determine whether the factor was caused by the deep drawing process, the process was studied by rotating the sheet to be drawn in three different orientations: 0° , 45° and 90° .

The result after deep drawing was a cup of 17.7 mm high.



Figure 2.9. Deep drawn cup

To study deep drawing, the blank was marked with a 0 in the rolling direction and the blankholder was also marked at one specific spot. In this way, to study the influence of deep drawing, the relative orientation between the 0 mark of the blank and the mark of the blankholder was alternated, forming 0° , 45° , and 90° . To control the tool-cup orientation, the tool was kept immovable in each of the repetitions and the mark of the cup was placed forming an angle of 0° , 45° or 90° relative to the mark of the deep drawing die.

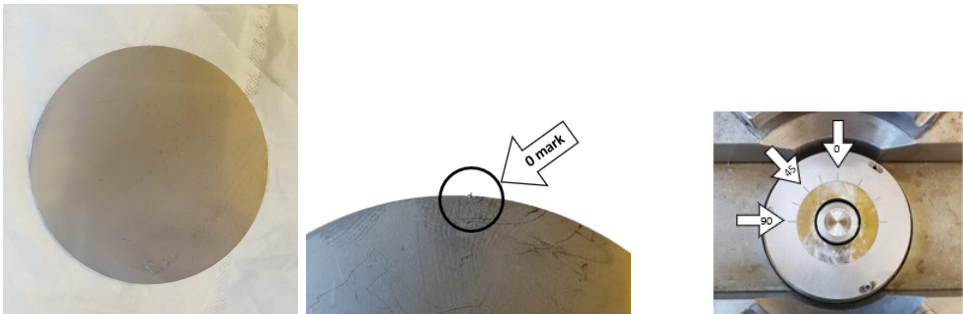


Figure 2.10. Laser cut metal sheet 1.4307 (left), 0 mark on the cup (center), and 0 mark on the deep drawing blank holder (right).

The sheets were first marked with its name: 'xXy' being x the angle formed between the rolling direction and L_0 , X the material (A=1.4404 or B=1.4307), and y the number of the repetition for the same deep drawing conditions (same material and same orientation).

Selected Tools

As it was wished to maintain as many variables as possible constant from Siimut's research, it was decided to use the same deep drawing machine, and same material and dimensions for the punch and the die. From [1, p.13], it was concluded that for 1 mm blank thickness, the punch-die clearance (Equation 1.1) should be about 1.22 mm, implying a punch diameter of 2.4 – 2.5 mm smaller than the die diameter. The tools used are:

- **The deep drawing machine:** Roell&Korthaus BP612 deep drawing machine, from 1961.
- **Punch:** diameter $\varnothing 32.6$ mm; nose radius 2 mm.
- **Die:** inner diameter $\varnothing 35.0$ mm; shoulder radius 2 mm.



Figure 2.11. Roell&Korthaus BP612 deep drawing machine.



Figure 2.12. a) Deep drawing punch, b) deep drawing die, c) deep drawing blankholder.

The stroke length of the deep drawing punch was set to 17.7 mm for all cups. The punch stroke was controlled manually by moving a lever, which may lead to deviations

for both the height and the flange size of the cup.

Friction

The process improves when increasing the friction between the blank and the punch, whereas friction between the top face of the blank sheet, the die and the blank holder must be reduced. To achieve this, lubricant Rhenus SU 500A was placed where required.

Speed of the punch

There is no mathematical expression to obtain the appropriate speed. Since the maximum speed that the deep drawing machine could achieve was 10 mm/s, a lower but efficient value was selected and kept constant for every repetition made. The speed of the punch was set to 1 mm/s.

Blank holder Force

According to Siimut's Thesis [1, p.94], the recommended blankholder force using Equation 1.6 should be $F_{BH} = 4.5$ kN for 1.4404 and $F_{BH} = 5.51$ kN for 1.4307. However, during experimentation he discovered that a higher blankholder force was required to eliminate wrinkling, needing 10.55 kN for 1.4404 and 6.33 kN for 1.4307. As it was wished to keep constant as many variables as possible during the development of the experiments, the F_{BH} chosen was the same for both materials. $F_{BH}=10.55$ kN was the force selected. As this was the correspondent value for sheets 1.4404, it was tested that it did not provoke fractures either wrinkle in sheets 1.4307.

The number of repetitions made depended on the results achieved. If the results after deep drawing different repetitions with the same experimental conditions were similar, then it could be concluded that the number of repetitions was sufficient to trust the results. The minimum number of repetitions per orientation and material was chosen to be three.

After deep drawing, the profile was measured using the CMM as explained in section 2.2.

The thickness distribution was obtained by subtracting the outer radius minus the inner. However, there was one problem when CMM measured the coordinates of these 500 points: the distance between two consecutive points were not the same for all the points in the circumference, meaning that one inner point and one outer point at the same row in the text file might not be the closest points. This created an error when subtracting the points row by row. To solve this problem the average polar coordinate of both inner and outer diameter was calculated every n degrees, and the average values of the radius were the ones subtracted.

| Inner polar coordinates | | Outer polar coordinates | |
|---------------------------|---------------------------|--------------------------|--------------------------|
| Angle (degrees) | Radius (mm) | Angle (degrees) | Radius (mm) |
| 8.9612916316733091358e+01 | 1.6436253291652999999e+01 | 8.824347407261399470e+01 | 1.729570610931990760e+01 |
| 9.036560220922129361e+01 | 1.643788300293056182e+01 | 8.898061627090569914e+01 | 1.729852823155603758e+01 |
| 9.110996463700719517e+01 | 1.643925684674886156e+01 | 8.970868183394482287e+01 | 1.729762034241231916e+01 |
| 9.184629887650639546e+01 | 1.644114874523673819e+01 | 9.041845832069209621e+01 | 1.729798689783741850e+01 |
| 9.256192413182851908e+01 | 1.644210031517372883e+01 | 9.114898435987261394e+01 | 1.729875134504193923e+01 |
| 9.327807934015470437e+01 | 1.644044555830588905e+01 | 9.187698209854455911e+01 | 1.729969191943665408e+01 |
| 9.40638288558409157e+01 | 1.644213427062785726e+01 | 9.259864457683593741e+01 | 1.729965688545083324e+01 |
| 9.479464391711714200e+01 | 1.644529886520489370e+01 | 9.333313104170464669e+01 | 1.730085200785249810e+01 |
| 9.553159688420154794e+01 | 1.644464492678758205e+01 | 9.406792802952587351e+01 | 1.730230474903664373e+01 |
| 9.627640768017825224e+01 | 1.644534362823370444e+01 | 9.477889135039906421e+01 | 1.730211428303090315e+01 |
| 9.701464138266800319e+01 | 1.6446886431866302456e+01 | 9.551030330844830019e+01 | 1.730541349503052828e+01 |
| 9.774625901716763110e+01 | 1.644822201601044398e+01 | 9.620042117413113658e+01 | 1.730423418334529373e+01 |
| 9.845974865794347863e+01 | 1.644958384169376231e+01 | 9.696492637338327825e+01 | 1.730617519876635768e+01 |
| 9.922152949568551605e+01 | 1.645092729366585971e+01 | 9.767656494990337990e+01 | 1.730852373589224413e+01 |
| 9.997530061544878777e+01 | 1.645225816064610314e+01 | 9.841330543186614932e+01 | 1.730893499619407550e+01 |
| 1.007084784439449834e+02 | 1.645437548048258947e+01 | 9.913110712149384085e+01 | 1.730957698514338361e+01 |
| 1.014520772562729860e+02 | 1.645533043568870113e+01 | 9.987510135842332204e+01 | 1.731201884113036016e+01 |
| 1.021802099705892317e+02 | 1.645746365413093315e+01 | 1.005770738322863167e+02 | 1.731203997005506778e+01 |
| 1.029225568463106413e+02 | 1.645769475457131392e+01 | 1.013135621096724890e+02 | 1.731401792483440971e+01 |
| 1.036694400842041972e+02 | 1.646010316731292278e+01 | 1.020378654944719443e+02 | 1.731638965961684207e+01 |

Figure 2.13. Text file showing the polar coordinates of the inner and outer diameters before calculating the average.

The example portrayed in Figure 2.13 shows how the closest points at 90° were not at the same row. The thickness calculation by hand in this case should be $17.29799 - 16.43788 = 0.86010$ mm at 90° (checked with Figure 4.20). It was chosen to calculate the average for $n=2^\circ$. To verify that the thickness distribution was properly calculated, one cup was chosen and thickness distribution was calculated by hand in different locations. It was achieved by saving the polar coordinates before calculating the average in a text file and subtracting by hand the outer and inner radius at the same angle. It was confirmed that these hand-calculated values matched the thickness distribution plot.

At the starting point of the project it was interesting to analyse the behaviour in the inner surface of the cup walls, so the CMM measurement plan for the first set of deep drawn cups did not measure the outer diameter. However, when the thickness distribution wanted to be calculated, the measurement plan was changed to also measure the outer diameter, but the first set of deep drawn cups had already been ironed. For this reason, new cups were deep drawn to measure also the outer profile with the new measurement plan. Therefore, the cups shown in the deep drawing results are not exactly the same cups as the cups shown in the ironing results.

Summary:

1. Deep draw a minimum of 9 laser cut sheets of 1.4307 (3 orientations x 3 repetitions) and 1.4404, rotating the relative orientation of the rolling direction with the deep drawing die from 0° , 45° and 90° .
2. Measurements in CMM: roundness of the inner and outer diameter at three different highs: 4 mm from the top, 6.5 mm and 10 mm.

3. Represent the corresponding roundness profile plot using the Python script.
4. Analyse the results.

2.4 Ironing

A similar experiment as deep drawing was conducted for ironing. Ironing was also studied by rotating the deep drawn cup in three different orientations: 0° , 45° and 90° relative to a mark in the ironing die, and the ironing die was always placed at the same spot and orientation relative to the subpress (see in Figure 2.16) . The punch was not moved or rotated at any time and its position was kept constant for every cup ironed.

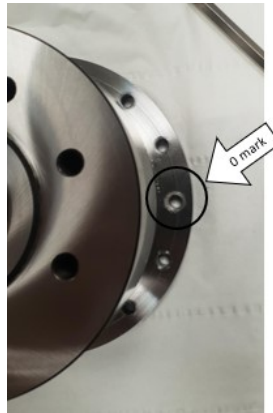


Figure 2.14. 0 mark on the ironing die

The ironing took place in a servo-mechanical press with maximum capacity of ± 150 kN, which includes a load cell (LC412-50K load cell of Omega Engineering, Inc.) to measure the axial punch force (kN), position (mm) and speed (mm/s). The tools selected were:

- **Adjustable punch:** Diameter $\varnothing 33.8$ mm; contact radius 10 mm.
- **Die:** Inner diameter $\varnothing 35.2$ mm; shoulder radius 2 mm.

The diameter of the punch was measured three times using a micrometer with a range of 25 – 50 mm and resolution of 1%. The instrument was calibrated using gauge blocks and the results of the calibration are shown in Figure 2.15.

In section 4.3 of Siimut's Thesis it was concluded that the mandrel extension force should not exceed 6.6 kN. Therefore, the torque selected should be in the range of 2–11 N m, what led to a mandrel extension force of approximately 1–5 kN. On the other hand, for too low ranges of the torque applied, the peak of the pressure

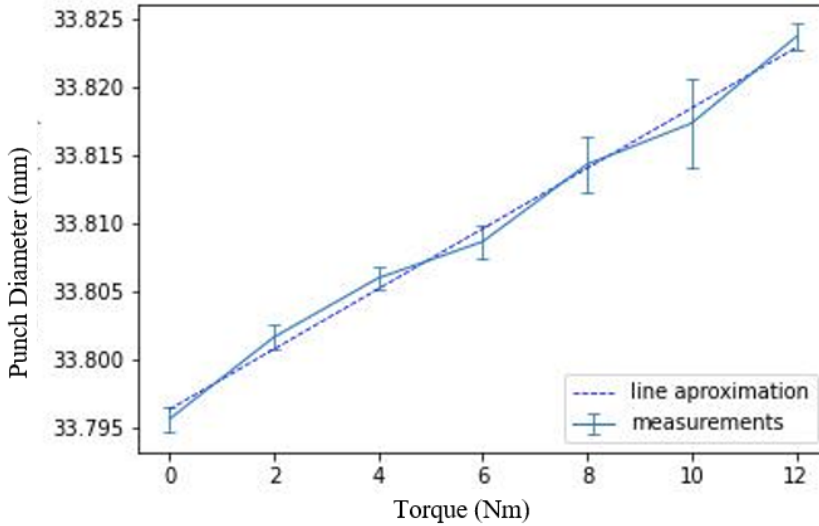


Figure 2.15. Diameter of the punch according to the torque applied to the mandrel. Curved line representing the average of the three measurements made, error bars representing \pm standard deviation and the dotted line represents the linear approximation of the measurements, $R^2 = 99.13\%$.

distribution on the punch-mandrel interface would likely be amplified [1, p.108]. Thus, 4 N m was selected as a low enough torque to avoid the high pressure at the tip of the mandrel.

To improve the alignment punch-die assembly a subpress was used. The subpress consisted of two horizontal plates and two columns surrounded by two compression springs SZ8010 50x254 [13]. Lateral movements were blocked by the fit between the columns and the bushings, which were mounted into the top plate [1, p. 68]. The force require to compress the springs had to be considered, since the force measured by the load cell was the force to iron plus the force applied to the springs. Therefore, the load of the springs must have been subtracted from the measured force to obtain the real ironing force:

$$F_{\text{measured}} = F_{\text{real}} + F_{\text{springs}} \rightarrow F_{\text{real}} = F_{\text{measured}} - F_{\text{springs}} \quad (2.2)$$

The force of the spring is obtained through Hooke's Law:

$$F_{\text{springs}} = k \cdot \Delta x + b, \quad (2.3)$$

where k is the elastic constant, Δx is the increment in length of the spring compared to its relaxed length, and b is the interception with the y -axis (initial force applied to compress the springs in the subpress). The elastic constant is provided by the manufacturer [13], being 35 N/mm. As there are two springs it could be assumed as

one single spring with $k=70$ N/mm. However, this value was calculated anyway. To obtain k and b , the load of the springs was measured through the whole stroke of the punch with no cup inside the die. The collected data was fitted to a straight line and both parameters were obtained (view in appendix 5).

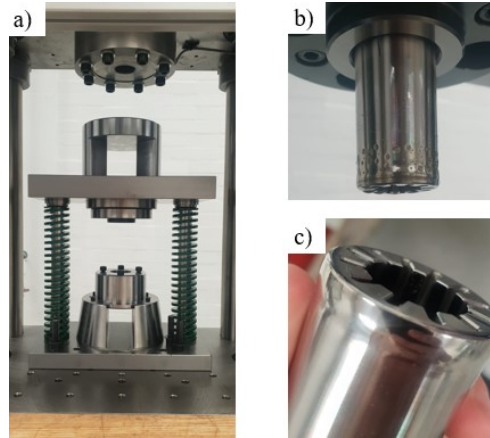


Figure 2.16. a) subpress, b) lubricated punch, c) punch with the mandrel retracted.

The steps to iron with an adjustable punch are found in Appendix G of Siimut's Thesis. The first step in the ironing procedure was to apply the lubricant (Rhenus SU 500A) to the die and all surfaces of the cup using a foam paint roller. Then cup was then placed into the die, and the blankholder was mounted. The blankholder screws were tightened until first resistance. With the help of another auxiliary servomechanical press, 140 kN was applied to the blankholder to effortlessly tight the eight screws up to 30 N m using a torque wrench. The ironing punch was then lubricated using the paint roller and additional lubricant was applied to the cup until covering the whole inner surfaces of the cup. Afterwards, the set die-blankholder is placed in the subpress stand using four M5x16 bolts. The punch is then moved to the zero-position (the top surface of the die) and the mandrel was extended applying the 4 N m torque previously selected. The mandrel was actuated by turning a M10x10 screw calibrated BTL-73 torque tool that had a torque range of 2 – 14 Nm and an uncertainty below 1%. By doing this the punch increased its diameter to approximately 33.81 mm. The punch speed was later set to 2 mm/s and stroke length to 16 mm for all specimens. Punch speed and end position were input to the control panel and forming stroke is performed. After the forward stroke the torque is released to 0 Nm and the screw of the mandrel is extracted a minimum of 720° , equivalent to raise the mandrel pitch 1 mm plus 1 mm of the actuator screw slack. Before starting the backstroke, about 1–2 ml of lubricant was injected between the punch shaft and blankholder around all the circular profile. At least 1 minute was waited to ensure that the whole surface was soaked off lubricant. Then, the final position was set in the control panel and again a speed of 2 mm/s to perform the backstroke [1, p.109]. To eject the cup, the ironing

die was placed on three steel blocks to clear up the path of ejection. The ejection is performed with the auxiliar press using an M14 (ISO 4762) screw with a plastic head cover as the ejector to protect the die surface. Excessive lubricant is then removed with a paper towel and finally cups are cleaned with an ethanol wipe.

Repetitions were considered valid when the plots for the same material, same orientation look alike. A minimum of three repetitions per orientation and material were conducted .

2.5 Tensile strength test procedure

To determinate the anisotropy of each material, EN 1.4404 and EN 1.4307, the tensile strength test was made under uniaxial load conditions.

The aim was to obtain the normal anisotropy in the 0° , 45° and 90° directions (R_0 , R_{45} and R_{90}) to determinate whether the material would deformed easily in one of these directions. A total of 30 tests were made, distributed in five tests per orientation and material.

The geometry of the specimens was cut according to DIN 50125:2009-07 [8].

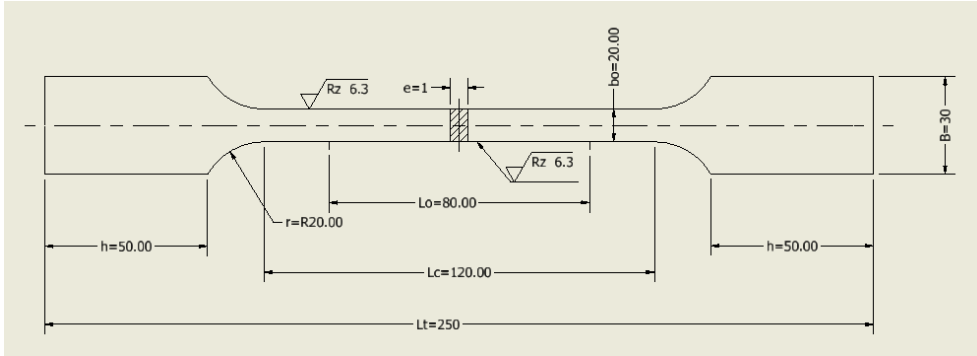


Figure 2.17. Geometry of sheets for the tensile strength test (mm) according to DIN 50125:2009-07.

where L_0 represents the original gauge length = 80 mm.

The machine used for the experiment is also a servo-mechanical press with maximum capacity of ± 150 kN. The sheet was first marked with each name: 'xXy' being x the angle formed between the rolling direction and L_0 , X the material (A=1.4404 or B=1.4307), and y the number of the repetition (0, 1, 2, 3 or 4). Then the specimen was placed in the grips and tied with the screws. To achieve an homogeneous force in each of the screws that held the specimen, the torque was controlled with a torque wrench set to 10 Nm, torque enough to tie the specimen during the test. Afterwards, the two extensometers were placed and plugged in the machine. Calibration certificates can be found in Appendix 5. The extensometers used were:

- Axial Extensometer, Epsilon technology corp, Model 3542-080M-050-ST, which measured the increase in length ΔL (mm).
- Transverse Extensometer, Epsilon technology corp, Model 3575-500M-ST, which measured the increase in width Δw (mm).

Where ΔL is defined as:

$$\Delta L = L - L_0 \quad (2.4)$$



Figure 2.18. Axial extensometer (left) and transverse extensometer (right)

The velocity of the press was set to 1 mm/s, and kept constant for all repetitions. The load applied (kN) and the extension for both extensometers (mm) was recorded in a text file every 10 ms. When fracture occurred the servo-mechanical press was stopped.

Once the data had been collected it was processed with a Python script (Appendix 5).

CHAPTER 3

Material Properties: Anisotropy

The R-value, or more accurately the vertical or normal anisotropy, is one of the typical characteristic values determined from tensile strength tests. According to the standard [8], to calculate the R-value, the true plastic width-strain and thickness-strain during uniform elongation need to be measured. However, it is easier to measure the increase in length than the change in thickness, therefore, assuming constant volume, the measured change in thickness can be computed as:

$$\epsilon_l + \epsilon_t + \epsilon_w = 0 \rightarrow \epsilon_t = -\epsilon_l - \epsilon_w \quad (3.1)$$

3.1 True stress-strain curve

Calculus to obtain the true stress

The engineering stress is defined as:

$$\sigma_N = \frac{F}{A_0}, \quad (3.2)$$

being F the load applied and A_0 the initial section ($A_0 = e_0 \cdot b_0$). The engineering stress and strain incorporates fixed quantities (the original not deformed measurements). Nevertheless, the section during the test is variable. True stress and true strain takes into account this variation of the section, using the instantaneous values of these dimensions, giving more accurate measurements. This is why to better analyse the properties of the material true values are used, and not engineering values [14].

To calculate the instant section the Equation 3.3 conforms,

$$A \cdot L = A_0 \cdot L_0 \rightarrow A = \frac{A_0 \cdot L_0}{L} \quad (3.3)$$

When the load starts to decrease after reaching its maximum value, necking starts and deformation is no longer homogeneous. For this reason, all the values collected after the maximum force were removed from the data frame.

Combining Equation 3.2 and Equation 3.3, the true stress is expressed as

$$\sigma_T = \frac{F}{A} = \frac{F \cdot (\Delta L + L_0)}{A_0 \cdot L_0} = \frac{F}{A_0} \cdot \left(\frac{\Delta L}{L_0} + 1 \right) \quad (3.4)$$

where all parameters are now known (A_0 and L_0 are initial values and F and ΔL are measured by the press).

Calculus to obtain the true strain

As the stress vector in the thickness direction can be considered close to 0, compared to the stress in the other two directions, tensile test in this case can be considered as planar stress. The equivalent strain in plane stress is the longitudinal strain ($\epsilon_{eq} = \epsilon_l$). See demonstration in Appendix 5.

A measure of the longitudinal strain takes the increment of strain to be the incremental increase in displacement dL divided by the current length L :

$$d\epsilon_L = \frac{dL}{L} \rightarrow \epsilon_L = \int_{L_0}^L \frac{1}{L} dL = \ln \frac{L}{L_0}, \quad (3.5)$$

where L is unknown, but can be obtained through Equation 2.4. Inserting (2.4) into (3.5) the true strain is finally acquired as:

$$\epsilon_L = \ln \left(\frac{\Delta L}{L_0} + 1 \right) \quad (3.6)$$

where now all the parameters are known (ΔL (mm) is recorded every 10 ms, and L_0 (mm) is the initial gauge length) [14].

The same equations apply to obtain ϵ_w .

True stress-strain curve

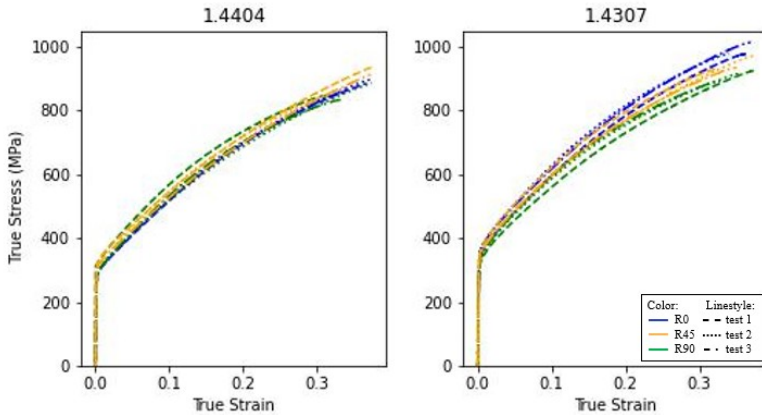


Figure 3.1. True stress-strain curve.

Although curves look alike and maximum values as well, stress-strain curves for 1.4404 are closer one for the other for the different orientations given.

3.2 R-value

Calculus to obtain the R-value

It was explained in section 1.4.1 the concept of R-value . From Equation 1.3, ϵ_w is unknown but can be obtained assuming constant volume (Equation 3.1).

R-values

Through the previous calculus the R-values were obtained for both materials the three orientations,

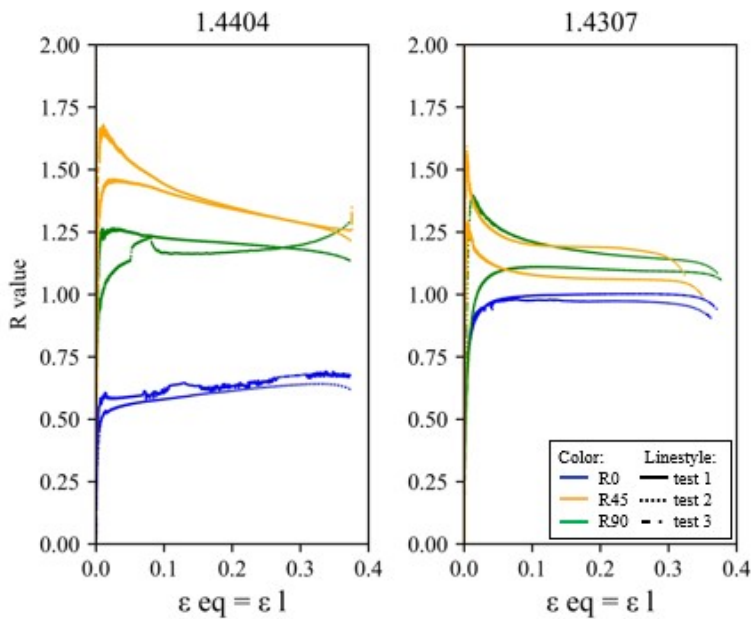


Figure 3.2. R-value of 1.4404 (left) and 1.4307 (right).

From the chart above it is clearly concluded that for EN 1.4404 $R_0 < R_{45} \approx R_{90}$: lower values of R_0 were obtained compared to R_{45} and R_{90} , which led to a more anisotropic behaviour.

However for EN 1.4307, mixed and similar values were achieved for the three orientations given, what could be translated as a less anisotropic material, and therefore, deformation may occur with the same ease in any direction.

To ensure that the R-value are properly calculated, R_0 of 1.4404 was also computed by hand, since it is the most constant value easier to determinate from the plots. In this way, the final width and final thickness was measured for three specimens and the R-value was obtained by:

$$R = \frac{\ln\left(\frac{w_f}{w_0}\right)}{\ln\left(\frac{t_f}{t_0}\right)}, \quad (3.7)$$

where w_f and w_0 are the final and initial width (mm) and t_f and t_0 are the final and initial thickness (mm).

The manual R-values obtained were all around 0.55, which approximately matched the R-value of the plot.

CHAPTER 4

Results and Discussion

4.1 CMM measurements of the tools

As mentioned before, the aim of this experiment was to discover any possible imperfection in the roundness of any of the tools used in the project.

4.1.1 Deep drawing die

The profile obtained for the inner diameter of the deep drawing die profile measured at two different heights (2.5 and 5.5 mm) was:

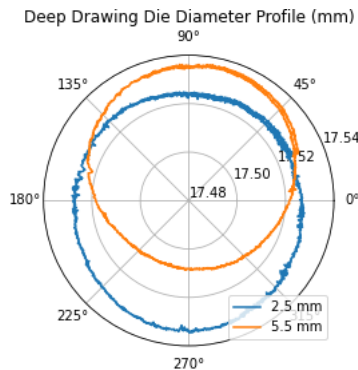


Figure 4.1. Deep drawing die roundness profile at 2.5 and 5.5 mm.

The first to be noticed was that the centers of the circumferences were not at the same location. It could be a misalignment in the CMM setup, but the deep drawing die was not moved while the measurement was performed and either the base alignment changed, what led to believe that it was a small bug in the tool that might have later caused a small dislocation in the deep drawing cup (off-center of around $18.7\ \mu\text{m}$): center of 2.5 mm was located at $(-0.00029, -0.00424)$ mm (Cartesian coordinates in the plane XY), whereas the center of 5.5 mm circumference was located at $(0.00204, 0.00143)$ mm, what implied a difference in the centers position of $18.7\ \mu\text{m}$.

Comparing this difference with the theoretical diameter of the deep drawing die (35 mm), it returned an off-center of 0.053%, which did not represent a significant value.

Furthermore, for 2.5 mm height, the difference in radius of the furthest and closest points was 12.74 μm . Knowing that the radius was 17.52 mm, it created an error of 0.0727%. On the other hand, for 5.5 mm height, the difference was 29.70 μm , which implied an error of 0.1695%.

In addition, roundness provided by the CMM software was 5.2 μm at 2.5 mm height and 4.3 μm at 5.5 mm height.

It was concluded that the deep drawing roundness at each height measured was within an acceptable range to consider that it would not create an elliptical roundness in the deep drawn cup (the relative error <1%, and roundness was <10 μm). Furthermore, there was no track of elliptical roundness in 1.4307 deep drawn cups, which meant that the deep drawing itself did not cause elliptical roundness.

4.1.2 Deep drawing punch

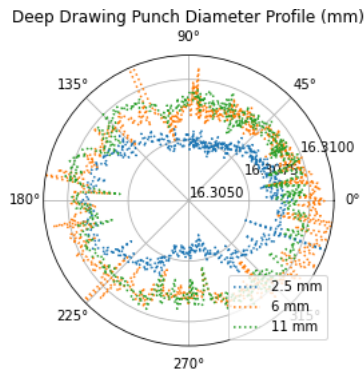


Figure 4.2. Deep drawing punch roundness at 2.5, 6 and 11 mm from the origin

It is to be noticed the elliptical shape that the clouds of points assumed. Nevertheless, it was later observed in results after deep drawing (4.2) that there was no elliptical track in 1.4307 deep drawn cups. This might have been perceived because of the reduced scale of the plot (the scale was set to represent a maximum of 5 μm).

Roundness given by CMM was in the range of 1.5 - 3 μm , except for the profile at 11 mm height where it was 7.7 μm .

4.1.3 Ironing mandrel (adjustable punch)

The mandrel, with its conical shape, was measured at four different heights: 0.5, 2.5, 4.5 and 6.5 mm, measured from the smallest circular flat plane at the end of the

conical section as pictured in Figure 2.3. It was decided to create four independent plots for each height, to better adjust the scale for each.

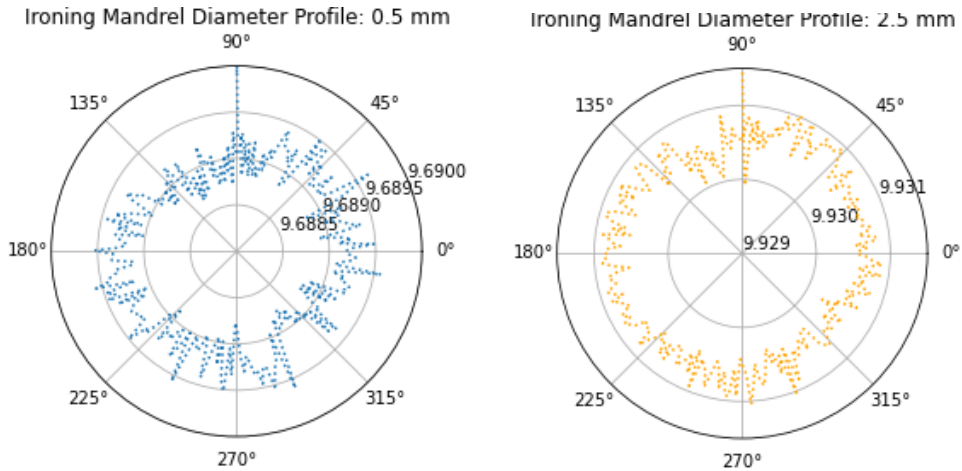


Figure 4.3. Roundness profile of the mandrel at 0.5 and 2.5 mm.

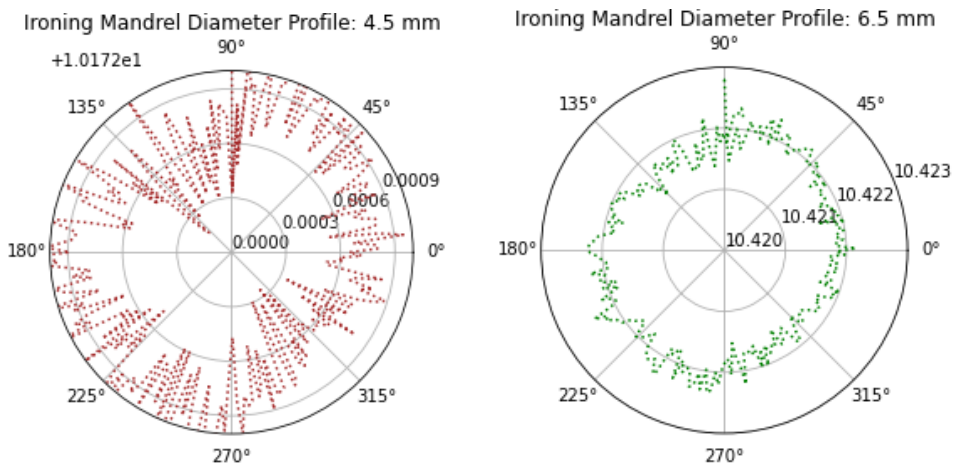


Figure 4.4. Roundness profile of the mandrel at 4.5 and 6.5 mm.

Although the graphs may not seem perfectly round, the scale must be considered. The first graph (at 0.5 mm height) represents a maximum radius of $1.5\ \mu\text{m}$, that compared to its diameter ($19.38\ \text{mm}$) led to an influence of $0.0015/19.38 = 0.0078\%$. Same occurred with the other heights: $2.5\ \mu\text{m}$ at 2.5 mm, $1.2\ \mu\text{m}$ at 4.5 mm,

and $3\text{ }\mu\text{m}$ at 6.5 mm . Thus, the results obtained show that the mandrel's diameters approached to an almost perfect circle. In addition, roundness obtained from the CMM was $0.9\text{ }\mu\text{m}$, $1\text{ }\mu\text{m}$, $0.9\text{ }\mu\text{m}$ and $1.1\text{ }\mu\text{m}$ for 0.5 , 2.5 , 4.5 and 6.5 mm heights respectively, what supported the previous statement. Therefore, it was concluded that neither the mandrel had a significant influence.

4.1.4 Ironing die

The results are plotted in Figure 4.5.

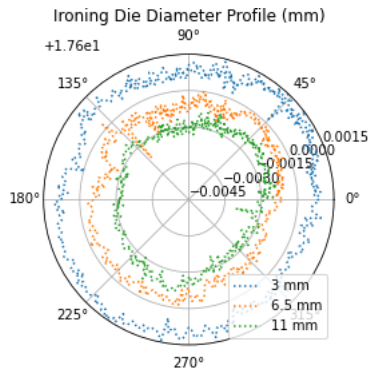


Figure 4.5. Ironing Die roundness profile at 4, 7.5 and 11 mm

The numerical roundness provided by the CMM software was $1.6\text{ }\mu\text{m}$, $2.4\text{ }\mu\text{m}$ and $1.6\text{ }\mu\text{m}$ for 4, 7.5 and 11 mm high respectively. What's more, the scale of this chart was set to only $6\text{ }\mu\text{m}$. It was proven then that the ironing die had an extreme precision in diameter and roundness.

4.1.5 Ironing punch

This was considered to be the most critical tool. Since the bimodal roundness appeared on cups ironed with an adjustable punch, it was conceivable that something occurred during the punch extraction with the mandrel retracted. Thus, the shape that the punch would have during said extraction was measured.

It was measured then, the diameter and roundness of the outer surface, measuring at the maximum of the torus (the punch nose).

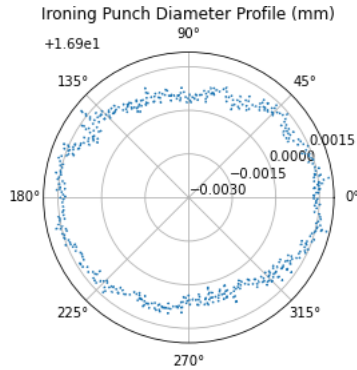


Figure 4.6. Ironing punch roundness profile (mm) at the maximum of the nose.

Although a slight elliptical shape seemed to appear, if it was the cause of elliptical roundness, this elliptical roundness of the ironed cups, it should have rotated in the plots (section 4.3) as the orientation of the cup was rotated in the ironing die. But it was not the case. The scale was set to represent $2.5\ \mu\text{m}$ which led to a deviation of 0.0074% comparing it with its diameter ($33.80\ \text{mm}$). In addition, roundness provided by CMM was $1.7\ \mu\text{m}$ which was a relative low value.

4.1.6 Conclusion

To be concluded, the plots have proven that the ironing tools are well-designed and well-manufactured. On the contrary, the deep drawing tools seem to have more imperfections, but non of them seem significant to obtaining bimodal roundness. Therefore, bimodal roundness must occur because of a specific property of the cups.

4.2 Deep drawing: roundness

The influence of the deep drawing was analysed. Only one cup is plotted per orientation. The other repetitions can be found in the Appendix 5.

4.2.1 1.4404

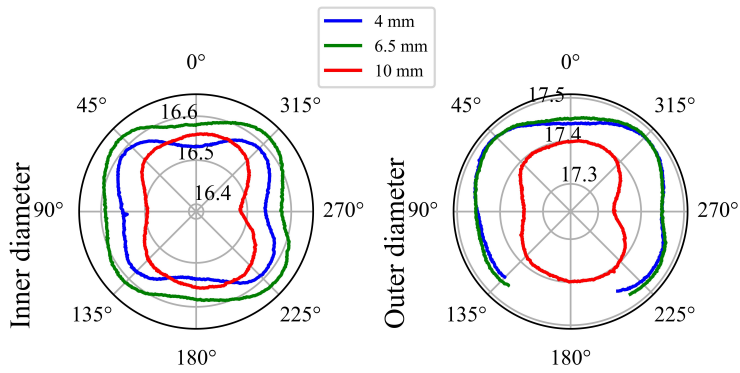


Figure 4.7. Deep drawing of 1.4404, 0° orientation, cup 3.

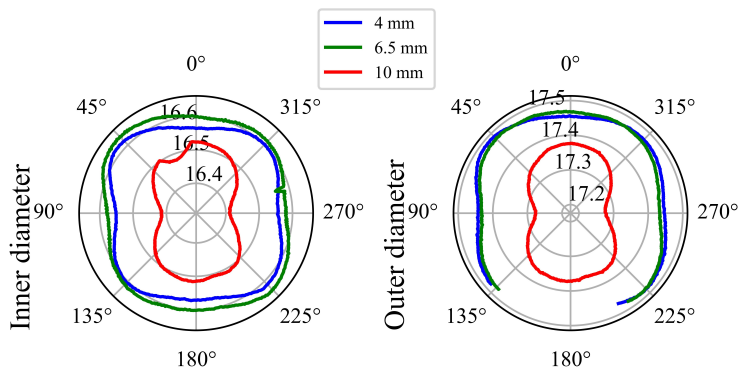


Figure 4.8. Deep drawing of 1.4404, 45° orientation, cup 4.

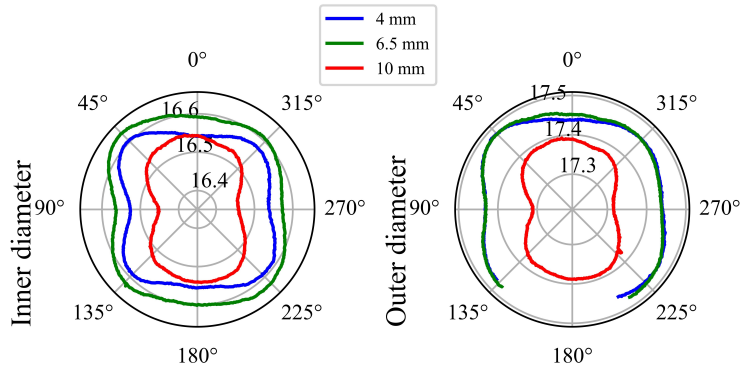


Figure 4.9. Deep drawing of 1.4404, 90° orientation, cup 5.

Roundness, no matter the orientation, was more likely to be round with small ears appearing at 45°. At 10 mm roundness may seem more elliptical. This is explained in section 4.3.3.

4.2.2 1.4307

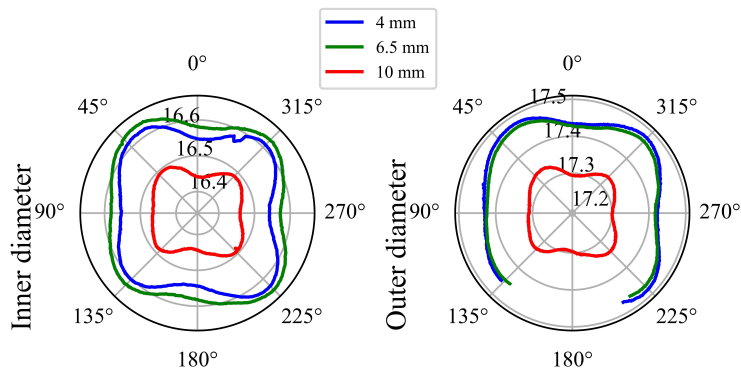


Figure 4.10. Deep drawing of 1.4307, 0° orientation, cup 6.

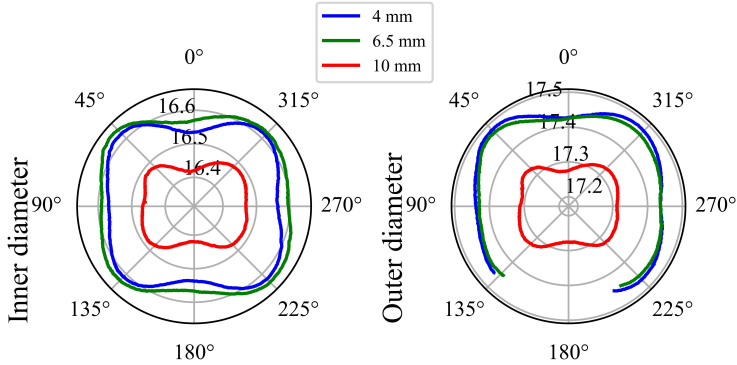


Figure 4.11. Deep drawing of 1.4307, 45° orientation, cup 4.

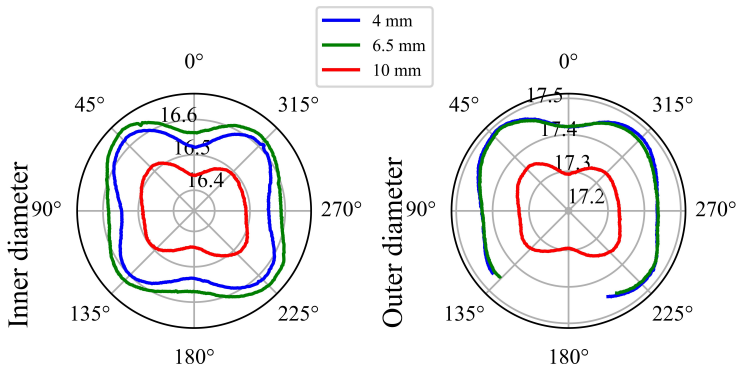


Figure 4.12. Deep drawing of 1.4307, 90° orientation, cup 0.

There was no track of an elliptical roundness but relative big ears appeared with its maximums every 45°. This meant that:

1. Bimodality was not caused by deep drawing.
2. As the maximums always appeared at the same location, $\pm 45^\circ$, it was caused by some property of the material, which needed to be explained.

As explained in section 1.4.1, when planar anisotropy is close to 0, the more that it indicates equal metal flow in all directions, eliminating the ears forming. On the contrary, when $\Delta r \neq 0$, big ears appear. For 1.4307, an approximation of planar anisotropy was $\Delta r(1.4307) = \frac{1+1.25-2 \cdot 1.6}{2} = -0.475 \neq 0$, which explained why ears appeared, and the reason why they appeared every 45° is that $R_{\max} = R_{45}$.

4.3 Ironing

4.3.1 Ironing punch force

The elasticity constant and the interception were calculated, obtaining $k = -0.6933 \frac{kN}{mm}$, but different values for the load moving down and the load moving up: $b_{\text{down}} = 68 \text{ kN}$, $b_{\text{up}} = 62 \text{ kN}$.

$$F_{\text{real}}(kN) = F_{\text{measured}}(kN) - \left(-0.6933 \frac{kN}{mm} \cdot \Delta x(mm) + 68 \text{ or } 62kN\right) \quad (4.1)$$

Similar to the force obtained in Figure 1.6, the load needed during the backstroke after retracting the mandrel and reducing the punch's stiffness and consequently its diameter, was almost a fifth of the load applied during the forming stroke. In addition, the force required to iron the cups was similar for both materials, and even more, similar for the three relative orientation of the rolling direction of the initial sheet and the ironing punch and die. Which meant that the relative orientation did not influence during the ironing process. Same was concluded previously with roundness.

The gap that appears in Figure 4.13 at 16 mm stroke occurs just when the mandrel was retracted.

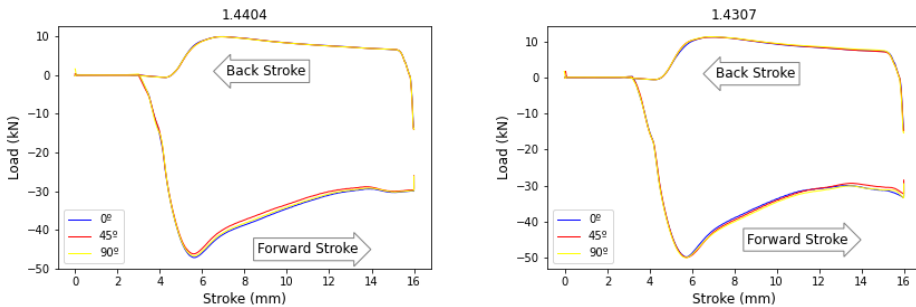


Figure 4.13. Ironing Punch Force 1.4404 (left) and 1.4307 (right) for each orientation.

4.3.2 Roundness

4.3.2.1 1.4404

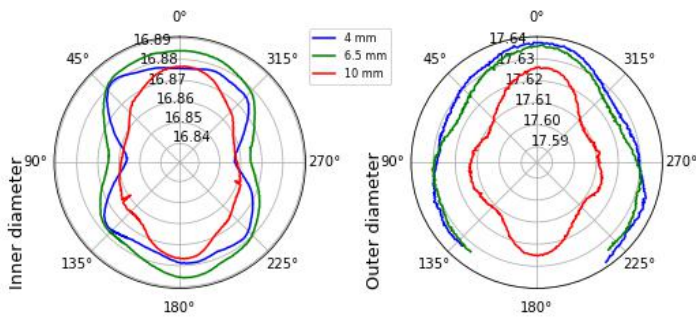


Figure 4.14. Ironing with adjustable punch of 1.4404 deep drawn cups, 0° orientation, cup 1.

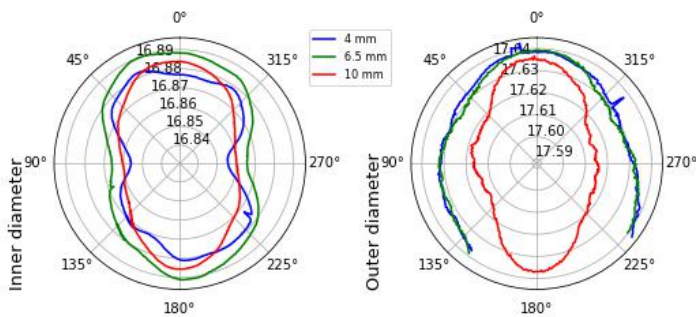


Figure 4.15. Ironing with adjustable punch of 1.4404 deep drawn cups, 45° orientation, cup 1.

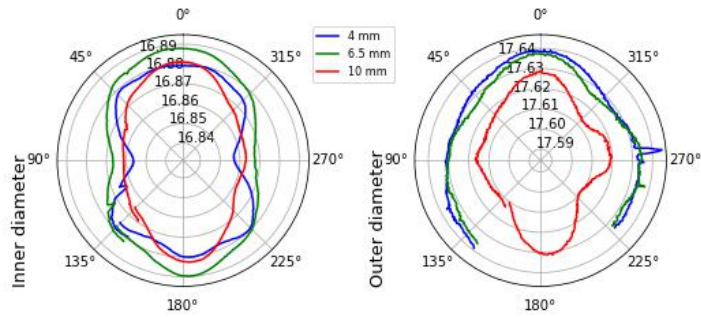


Figure 4.16. Ironing with adjustable punch of 1.4404 deep drawn cups, 90° orientation, cup 1.

It is seen in the graphs that a clear elliptical profile was found with its larger diameter in the rolling direction.

4.3.2.2 1.4307

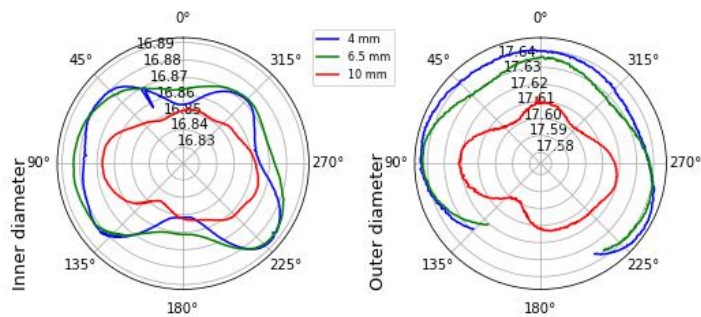


Figure 4.17. Ironing with adjustable punch of 1.4307 deep drawn cups, 0° orientation, cup n^o2.

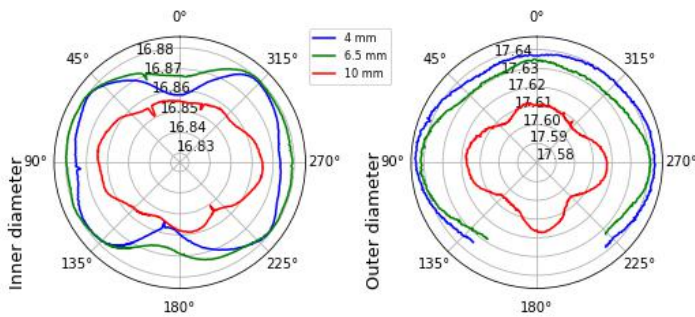


Figure 4.18. Ironing with adjustable punch of 1.4307 deep drawn cups, 45° orientation, cup n°1.

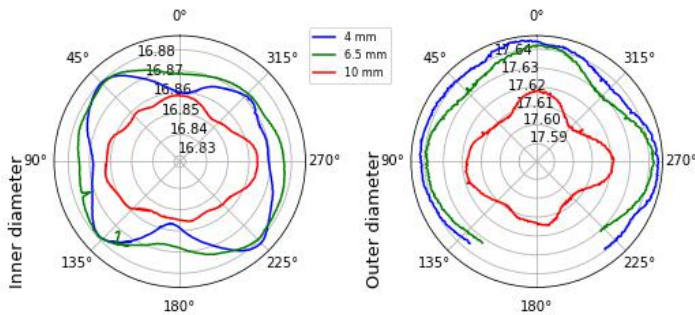


Figure 4.19. Ironing with adjustable punch of 1.4307 deep drawn cups, 90° orientation, cup n°2.

For 1.4307, more "random" distributions were achieved and there was no perception of an elliptical pattern. As this was a less anisotropic material, it made sense that there was no deformation in any preferential direction.

4.3.3 Discussion

From the differences observed when ironing both materials it could be said that it was not ironing with the adjustable punch what created the bimodal roundness in the profile of the cup, but the anisotropy of the material that was ironed with the adjustable punch.

The reason why the anisotropy affected when ironing with the adjustable punch but not with the conventional punch was that when retracting the mandrel, the punch reduced its stiffness and adapted more easily to the surrounds.

The question to be answered was why after ironing 1.4404, an ellipse appeared showing its greater diameter in the rolling direction. To answer this question, the thickness distribution of the deep drawn cup was studied in detail.

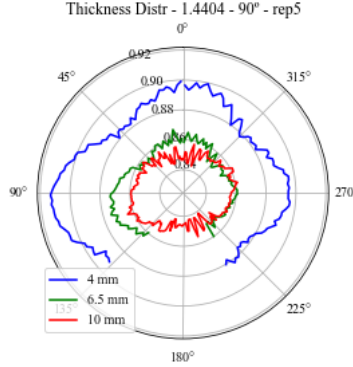


Figure 4.20. Thickness distribution of a deep drawn cup.

From Figure 4.20 it is observed that in the plane at 10 mm depth, the cup was thinner at 0° and thicker at 90° . The position of the punch when the mandrel is retracted is near this 10 mm plane. Therefore, the punch would fit this thickness distribution when the mandrel was retracted and as a consequence, an elliptical shape was caused in the backstroke. The reason why this occurred is based on the R-value obtained in section 3.2.

In the case of rigid-plasticity, not Hooke's Law but the flow rule applies. In addition, it can be considered plane stress since the stress applied in the z direction (thickness direction of the flat sheet) was the blankholder pressure, but since this was such a small value compared to the radial and tangential stress it could be neglected. Hence, it could be assumed to be plane stress ($\sigma_z = 0$).

Flow rule in plane stress:

$$\frac{d\epsilon_\theta}{1 + R - R \cdot X} = \frac{d\epsilon_r}{(1 + R)X - R} = \frac{-d\epsilon_z}{1 + X} \Rightarrow \frac{d\epsilon_\theta}{1 + R - R \cdot X} = \frac{-d\epsilon_z}{1 + X} \quad (4.2)$$

where X is the ratio between the radial stress and the tangential stress ($X = \frac{\sigma_r}{\sigma_\theta}$).

Considering first in the **outer radius**, in a free surface, $\sigma_r = 0 \Rightarrow X = 0$. Inserting

this in (4.2),

$$\begin{aligned}
 X = 0 &\Rightarrow \frac{d\epsilon_\theta}{1+R} = -d\epsilon_z \\
 \frac{d\epsilon_\theta}{1+R} &= -d\epsilon_z \Rightarrow \\
 d\epsilon_z &= \frac{-1}{1+R} \cdot d\epsilon_\theta
 \end{aligned} \tag{4.3}$$

For the own characteristic of the deep drawing process, the tangential strain $d\epsilon_\theta$ is per definition negative at the flange surface, which converts the z strain into positive.

A high R-value in Equation 4.3 implies that regions with higher R would have smaller thickness strain than regions with lower R.

Otherwise, at **any radius within the flange**, $\sigma_r > 0, \sigma_\theta < 0 \Rightarrow X < 0$. Inserting this in (4.2) :

$$\begin{aligned}
 \frac{d\epsilon_\theta}{1+R-R \cdot X} &= \frac{-d\epsilon_z}{1+X} \Rightarrow \\
 d\epsilon_z &= \frac{-(1+X)}{1+R(1-X)} \cdot d\epsilon_\theta
 \end{aligned} \tag{4.4}$$

By increasing R in Equation 4.4, the same conclusion was achieved as increasing R when studying outer radius : $|d\epsilon_\theta| > |d\epsilon_z| \Rightarrow$ higher deformation in the width than in thickness occurred when increasing R-values. Therefore, the final conclusion was that regions with high R suffered smaller thickness strain than regions with lower R-values, and as a consequence there was less thickness reduction and walls were thicker where the R-values were higher. On the contrary, in regions with low R-values, walls became thinner.

Relating this theoretical conclusion with the R-values of 1.4404 obtained in the tensile strength test in section 3.2, where $R_0 < R_{45} \approx R_{90}$, thickness strain at 0° (where R is lower) was bigger than the regions at 45° and 90° , and therefore the final thickness at 0° was thinner than the other regions.

CHAPTER 5

Conclusions and Further Research

By the CMM measurements of the tools and the results obtained with the rotation of the cups when deep drawing and ironing, it was found that no tool involved in the metal forming processes caused the bimodal roundness in the cups.

Furthermore, although Siimut's results showed that bimodal roundness appeared when ironing with the adjustable punch but not with the conventional punch, it was found that elliptical roundness did not emerge from every ironing operation with adjustable punch, but when ironing more anisotropic materials. Therefore, the less anisotropic behaviour a material has, the less connection between bimodal roundness and the use of the adjustable punch. Or in other words, the more anisotropic the material is, the more tendency to generate bimodal roundness after deep drawing.

Through the rigid-plasticity in plane stress theory, it was proved that lower R-values in one direction compared to the others, the thinner the walls of the cup would become after deep drawing in that region, and as consequence, the punch would later fit, after retracting the mandrel at the end of the forming stroke, the thickness distribution of the cup at that position.

Different experiments may be conducted to support and enrich the conclusions achieved in this project. One possible experiment would be to repeat the procedure followed in this thesis, but now with two different materials, one more isotropic, such as aluminium, and another more anisotropic. For the different materials used, some parameters would need to be re-calculated, such as the blankholder pressure, the punch-die clearance or the LDR, among others. In this way, the isotropic material should follow similar results as the results achieved for 1.4307 (no clear pattern in roundness after ironing with the adjustable punch), whereas the results of the more anisotropic material should be similar as the conclusion achieved for 1.4404: bimodal roundness is achieved, with its higher diameter in the direction where the R-value is lower.

Anisotropy in other directions, such as 30° and 60° , could also be studied in the tensile strength test and obtain the vertical and planar anisotropy at each direction. Thus, it would be verified whether for 1.4404, the lower R-value is obtained at 0° , and for 1.4307 it would be confirmed that it is a more isotropic material and no higher or

lower value is obtained at 30° or 60° .

Another interesting experiment could be designed. If found a way to make it possible, it would be intriguing to measure the inner and outer diameter of an ironed cup just right after the forming stroke and analyse the roundness and thickness distribution at this stage. This experiment is tough to design since it is not possible to extract the cup from the ironing assembly unless the punch has been retracted. The only possible way to achieve this would be to be able to extract the cup without performing the backstroke, and this could be achieved by reducing the punch diameter after the forward stroke within a range so that it would no longer touch the cup walls.

Bibliography

- [1] K. Siimut, *Development of a Novel Metal Forming Punch with Adjustable Diameter*. Master's Thesis, Department of Civil and Mechanical Engineering, DTU, 2022.
- [2] Thyssenkrupp, "Stainless Steel 1.4404," <https://ucpcdn.thyssenkrupp.com/legacy/UCPthyssenkruppBAMXUK/assets/files/material-data-sheets/stainless-steel/stainless-steel-1.4404-316l.pdf>, (accessed:05.06.2023).
- [3] Thyssenkrupp, "Stainless Steel AISI 304L 1.4307," <https://www.thyssenkrupp-materials.co.uk/stainless-steel-304l-14307.html>, (accessed: 05.06.2023).
- [4] A. Alaswad, K. Benyounis, and A. Olabi, "Optimization techniques in material processing," in *Reference Module in Materials Science and Materials Engineering*, Elsevier, 2016.
- [5] M. P. Groover, *Fundamentals of Modern Manufacturing*. 5th Edition.
- [6] T. Altan and A. E. Tekkaya., *Sheet Metal Forming - Fundamentals*. 1st ed., ASM International, 2012.
- [7] E. Doege, T. Hallfeld, Y. Khalfalla, and K. Benyounis, "Metal working: Stretching of sheets," in *Reference Module in Materials Science and Materials Engineering*, Elsevier, 2016.
- [8] German Institute of Standardization, *Testing of Metallic Materials - Tensile Test Pieces*. DIN 50125:2009-07, 2009.
- [9] CV Nielsen and N Bay, *Sheet materials*. Course material for 41730 Industrial forming of metals., Technical University of Denmark, 2022.
- [10] C. Nielsen, Ú. Arinbjarnar, E. Ceron, T. Madsen, B. Møller, K. Madsen, and K. Siimut, "A novel ironing punch concept with adjustable tool diameter," *CIRP Annals - Manufacturing Technology*, 2023.
- [11] J. L. D. Z. Marciniak and S. J. Hu., *Mechanics of Sheet Metal Forming*. 2nd ed, Oxford: Butterworth-Heinemann, 2002.

- [12] Varius authors, “Least squares circle,” <https://scipy-cookbook.readthedocs.io/items/Least-Squares-Circle.html>, (accessed: 16.04.2023).
- [13] STEINEL, “system springs catalogue,” <https://www.steinell.com/fileadmin/user-upload/STEINEL-catalogue-springs-system-springs-en.pdf>, (accessed: 16.05.2023).
- [14] Z. Marciniak, J. Duncan, and S. Hu, “1 - material properties,” in *Mechanics of Sheet Metal Forming (Second Edition)* (Z. Marciniak, J. Duncan, and S. Hu, eds.), pp. 1–13, Oxford: Butterworth-Heinemann, second edition ed., 2002.
- [15] Daniele Cozzolino, “Overleaf Template: DTU Fotonik: a PhD Thesis,” 2020, <https://www.overleaf.com/latex/templates/dtu-fotonik-a-phd-thesis/tsjsfpxkxgzw>, (accessed:21.05.2023).
- [16] “DTU Logo,” <https://leakagemanagement.net/partner/dtu/>, (accessed:03.06.2023).

Appendices

Python Scripts

The Python scripts only show how the data was processed, but not the lines of the code where the plots were generated.

Roundness of the cups

Deep drawn and ironed cups, CMM coordinates: least squares and translation to (0,0):

```
#Roundness.py
import pandas as pd
import numpy as np
import math
import matplotlib.pyplot as plt
from scipy.optimize import least_squares

def circle(c, X, Z):
    return ((X - c[0])**2 + (Z - c[2])**2 - c[1]**2)**2

def centerCircle(X,Y,Z):
    #Least Squares:
    res = least_squares(circle, [0, 1, 0], args=(X, Z))
    c = res.x
    return c

def toPolar(u,w):
    #Convert to polar
    n=len(u)
    polar=np.empty((n,2))
    minr=100
    maxr=0
    for i in range(n):
        xp=u[i]
        zp=w[i]
```

```

    #Angle (Degrees)
    angle=math.atan(zp/xp)
    if(xp>0 and zp>0):
        theta=angle
    elif(xp<0 and zp>0):
        theta=angle-math.pi
    elif(xp<0 and zp<0):
        theta=angle-math.pi
    elif(xp>0 and zp<0):
        theta=2*math.pi+angle
    polar[i,0]=theta-math.pi/2

    #Radius
    r=math.sqrt(xp**2+zp**2)
    polar[i,1]=r
    if r>maxr: maxr=r
    if r<minr: minr=r

    return polar, minr, maxr

def Translacion(X,Z,d):
    #Transladata the center and the points to (0,0)
    u=X+d[0]
    w=Z+d[2]
    return u,w

def loadData(filename):
    #Open files and create a vector with each file
    data=pd.read_csv(filename,header=None,sep=" ",dtype=float)
    X=data.iloc[:,0]
    Y=data.iloc[:,1]
    Z=data.iloc[:,2]
    c0=[0,0,0]
    c=centerCircle(X,Y,Z)
    d=c0-c
    #u, v are the translation of x and z coordinates to the center chosen.
    u,w=Translacion(X,Z,d)
    return toPolar(X,Z)

```

Thickness distribution of the cups

```

#Thickness distribution.py
import pandas as pd
import numpy as np
import math
import matplotlib.pyplot as plt
from scipy.optimize import least_squares
from roundness import circle
from roundness import centerCircle
from roundness import loadData
from roundness import toPolar

def polarSorted(f0):
    #Sorts the polar coordinates by angle (in degrees)
    #load data
    polar, maxr, minr, c =loadData(f0)
    #convert to degrees
    polar[:,0]= abs(polar[:,0]*180/math.pi)
    #sort according to the angle
    polar = sorted(polar, key=lambda x: x[0])
    #transform into a matrix
    polar = np.matrix(polar)
    return polar, c

def averageCalculation(polar, n):
    #Calculates de average polar coordinate every n degrees.
    N=math.trunc(360/n)
    average=np.zeros((N,2))
    for i in range(0, 360, int(n)):
        c=0
        sum_angles=0
        sum_radius=0
        for j in range(len(polar)):
            if (i<=polar[j,0]<i+n):
                #print(polar_i[j,0])
                sum_angles += polar[j,0]
                sum_radius += polar[j,1]
                c += 1
        if c>0:
            a=math.trunc(i/n)
            #print(sum_angles_i, sum_radius_i, c)
            average[a,0]=sum_angles/c

```

```

        average[a,1]=sum_radius/c
    return average

def thicknessCalculation(average_i, average_o, n):
    #Calculates the thickness distribution
    N=len(average_i)
    thickness = np.zeros((N,2))
    for i in range(0, 360, n):
        a=math.trunc(i/n)
        ri=average_i[a,1]
        ro=average_o[a,1]
        if (average_o[a,0]>0): #excludes angles with no outer point.
            # 1. Calculate the average angle evary n=2 degrees.
            thickness[a,0] = ((average_i[a,0]+average_o[a,0])/2)
            # 2. Distance between radius
            d=ro-ri
            thickness[a,1] = d
    return thickness

def deleteThickness(thickness):
    #Delete rows with no outer point recorded.
    c=0
    m=len(thickness)
    for i in range(m):
        if (thickness[i-c,0]==0):
            thickness=np.delete(thickness, i-c, axis=0)
            c += 1
    for i in range(len(thickness)-1):
        if thickness[i+1,0]-thickness[i,0] > 10:
            stop = i
    return thickness, stop

```

Springs of the subpress

```

def loadcsv(f0):
    #Load data
    df = pd.read_csv(f0, sep =";")
    return df

def cleanData(f0):
    #Load data
    df = loadcsv(f0)

```

```

#TIME
n = len(df)-1
time= df.loc[n, 'TIME [ms]']

#CLEAN DATA
del df['ROWIDX']
del df['TIME [ms]']
del df['TIME [HH:MM:SS.nnn]']
del df['EXTENSO [mm]']
del df['TRANS_EXTENSO [mm]']
del df['VEL_AXIS_A [mm/s]']
del df['VEL_AXIS_B [mm/s]']
#Me quedo con: A, B, Load

#Rename important columns
df = df.rename(columns={'LOAD_CELL [kN]': 'Load', 'POS_AXIS_A [mm]': 'A'})
df = df.rename(columns={'POS_AXIS_B [mm]': 'B'})

return df, time

def processData(f0):
    #Load and Clean Data
    df, time = cleanData(f0)

    #Stroke
    df['Stroke'] = -((df['A'] + df['B'])/2 - 948.9)
    df['Springs Ax'] = (df['A'] + df['B'])/2

    #k and b values (b changes for the up and down stroke)
    k=-0.06933
    if f0[0]=='0':
        if f0[4]=='u':
            b=62
        else:
            b=68.22242079
    else:
        if f0[5]=='u':
            b=62
        else:
            b=68.22242079

    df['Springs Load'] = k*df['Springs Ax'] + b

```

```

#Real Load (Load - Spring Load)
df['Real Load'] = -(df['Load'] - df['Springs Load']) #o springs_data.['Load']
return df, time

```

Ironing punch force

```

def cleanData(f0):
    #Load data
    df = pd.read_csv(f0, sep =";")

    #TIME
    n = len(df)-1
    time= df.loc[n, 'TIME [ms]']

    #Rename important columns
    df = df.rename(columns={'LOAD_CELL [kN]': 'Load', 'POS_AXIS_A [mm]': 'A'})
    df = df.rename(columns={'POS_AXIS_B [mm]': 'B'})
    return df

def processData(f0):
    #Load and Clean Data
    df = cleanData(f0)

    #Stroke
    df['Stroke'] = -((df['A'] + df['B'])/2 - 948.9)
    df['Springs Ax'] = (df['A'] + df['B'])/2

    #Springs
    k=-0.06933
    #Values of interception (up and down)
    if f0[0]=='0':
        if f0[4]=='u':
            b=62.66828073
        else:
            b=68.22242079
    else:
        if f0[5]=='u':
            b=62.66828073
        else:
            b=68.22242079

```



```

df['Springs Load'] = k*df['Springs Ax'] + b

#Real Load (Load - Spring Load)
df['Real Load'] = -(df['Load'] - df['Springs Load'])

return df

```

Tensile strength test

```

def loadcsv(f0):
    #Load data
    df = pd.read_csv(f0, sep =";")
    return df

def cleanData(f0):
    #LOAD DATA
    df = loadcsv(f0)

    #Rename columns
    df = df.rename(columns={'EXTENSO [mm]': 'A1', 'TRANS_EXTENSO [mm]': 'Aw'})
    df = df.rename(columns={'LOAD_CELL [kN]': 'Load'})
    #Al (variación de L); At (variación de t)

    #Initial Values
    Alo = df.loc[0, 'A1']
    Awo = df.loc[0, 'Aw']
    time_o = df.loc[0, 'TIME [ms]']
    Fo = df.loc[0, 'Load']

    #Time
    n = len(df)-1
    time_f = df.loc[n, 'TIME [ms]']
    time = ((time_f - time_o)/1000).round(1) #s

    #Delete last rows (after fracture)
    mask = (df.index >= 100) & (df['Load'] > -5)
    filas_a_eliminar = df[mask].index
    df = df.drop(filas_a_eliminar)

```

```

#Delete the rows when the axial extensometer reached its limit (36.35 mm)
df=df.drop(df[df['A1']>=36.3490].index)
return df, Fo, Alo, Awo, time

def processData(f0):
    #Load and Clean Data
    df, Fo, Alo, Awo, time = cleanData(f0)
    Lo=80
    b=19.12
    e=1

    #subtract initial values
    df['Load'] -= Fo
    df['A1'] -= Alo
    df['Aw'] -= Awo

    #Longitudinal and width strain
    df['el'] = np.log(df['A1']/Lo+1)
    df['ew'] = np.log(df['Aw']/b+1)

    #Thickness Strain
    df['et'] = 0 - df['el'] - df['ew']

    #R value
    df['R'] = (df['ew']/df['et'])

    #True Stress (MPa)
    Ao=b*e
    #Stress = F/A = F/(Ao*e-el) x1000 (Mpa)
    df['True Stress'] = abs(df['Load'])*(df['A1']/Lo+1)/Ao*1000

    #Delete right after necking
    necking = df['True Stress'].idxmax()
    df = df.drop(df[df.index >= necking].index)

    #True Strain
    df['True Strain'] = df['el']

    return df, time

```

Additional CMM Measurement of the Cups

Deep drawing

1.4404

0° orientation

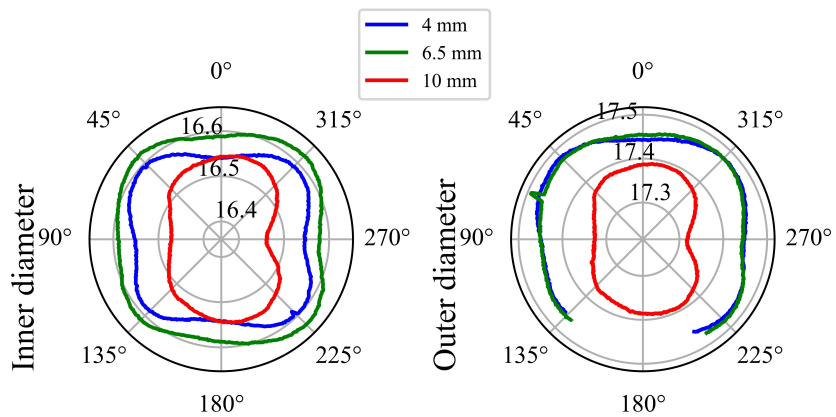


Figure 1. Deep drawing, 1.4404 blank, 0° orientation, cup 4

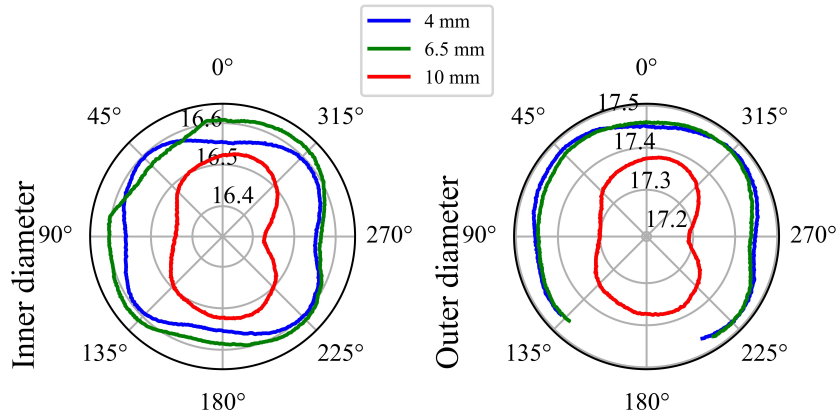


Figure 2. Deep drawing, 1.4404 blank, 0° orientation, cup 5

45° orientation

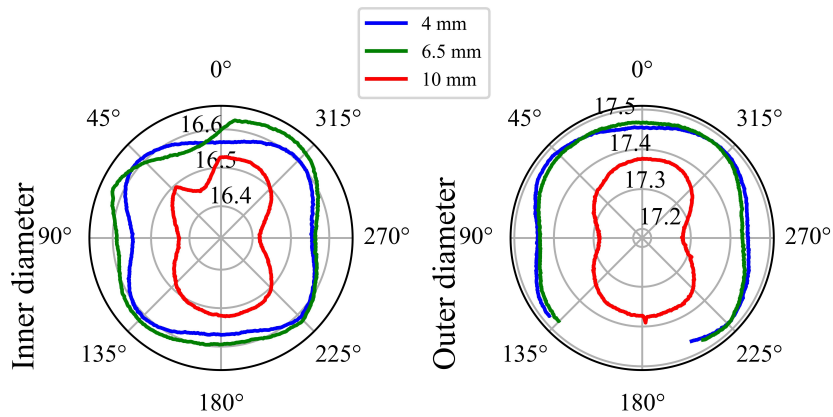


Figure 3. Deep drawing, 1.4404 blank, 45° orientation, cup 3

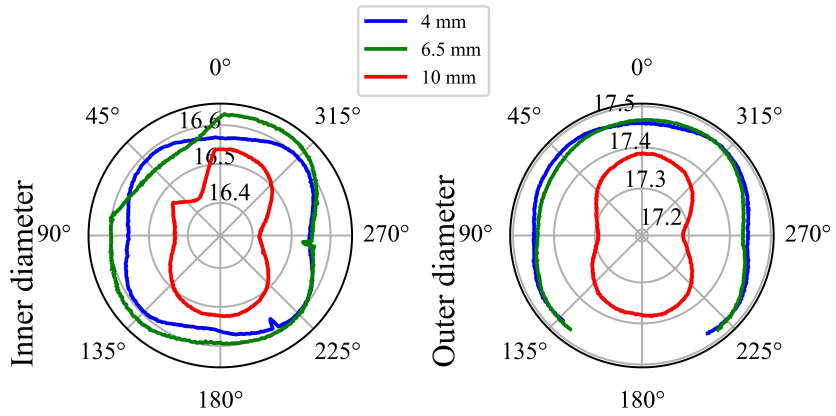


Figure 4. Deep drawing, 1.4404 blank, 45° orientation, cup 6

90° orientation

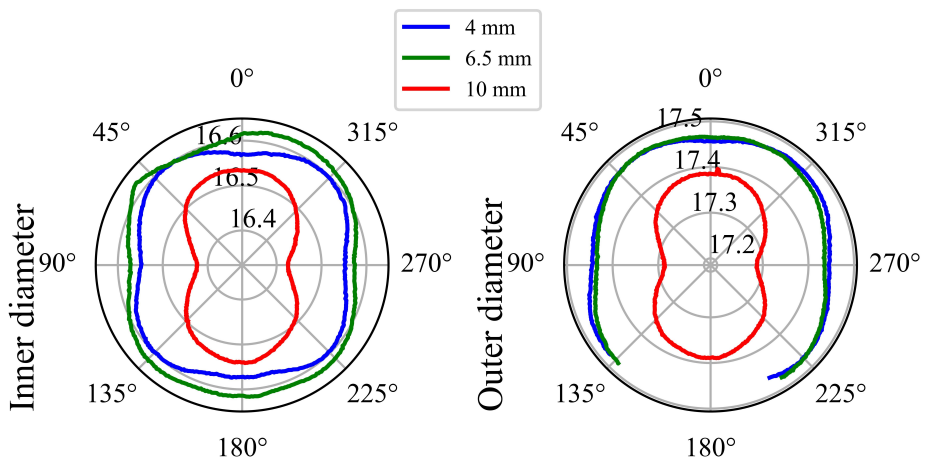


Figure 5. Deep drawing, 1.4404 blank, 90° orientation, cup 3

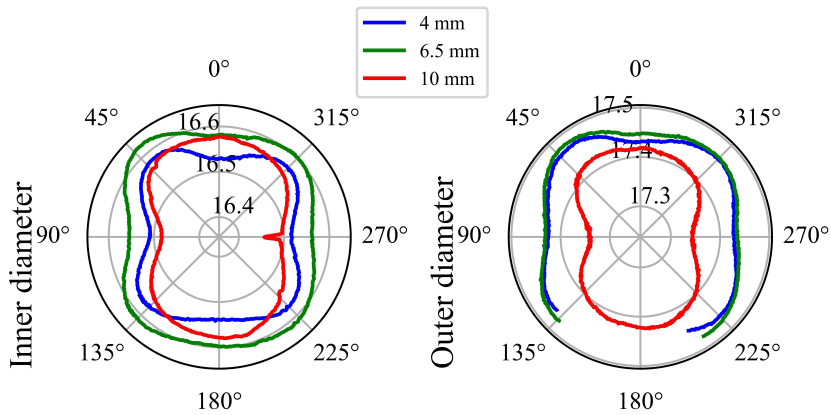


Figure 6. Deep drawing, 1.4404 blank, 90° orientation, cup 4

1.4307

0° orientation 45° orientation 90° orientation

Ironing

1.4404

0° orientation 45° orientation 90° orientation

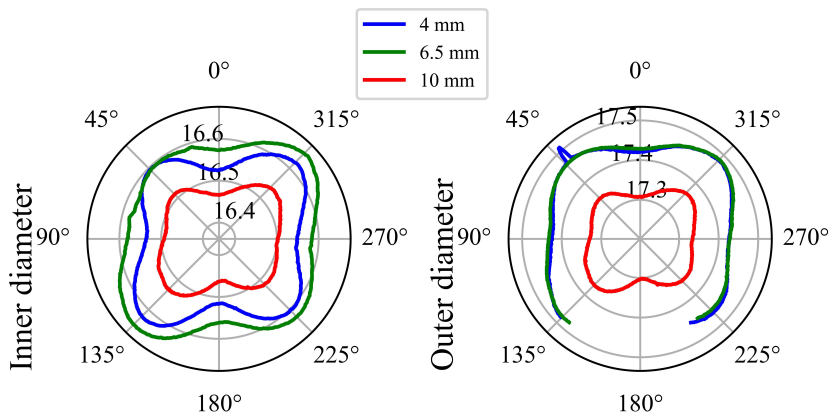


Figure 7. Deep drawing, 1.4307 blank, 0° orientation, cup 0

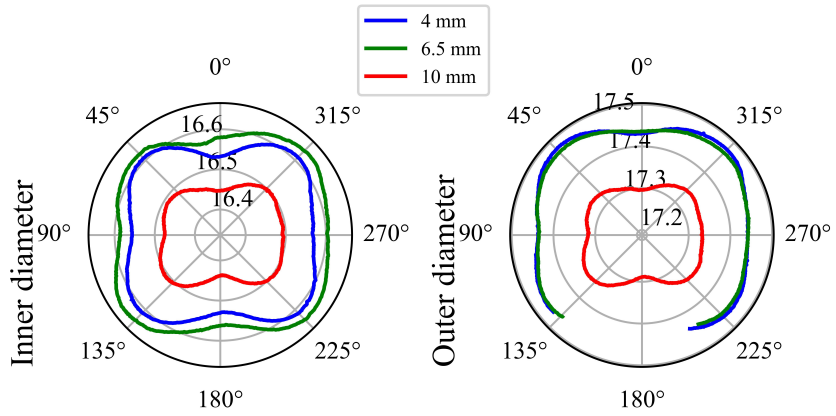


Figure 8. Deep drawing, 1.4307 blank, 45° orientation, cup 0

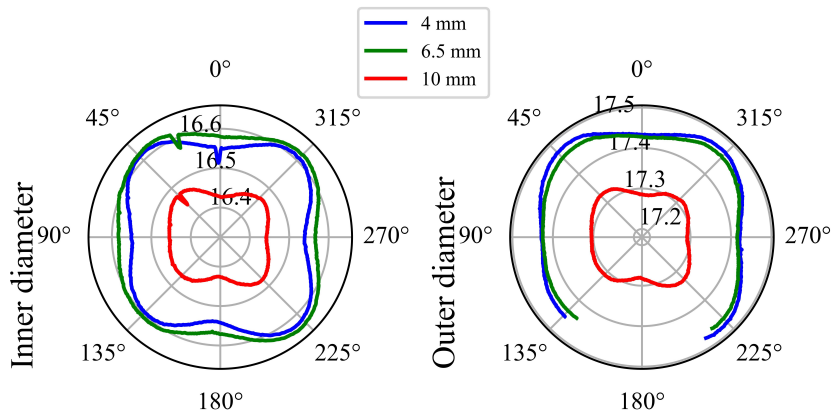


Figure 9. Deep drawing, 1.4307 blank, 45° orientation, cup 5

1.4307

0° orientation 45° orientation 90° orientation

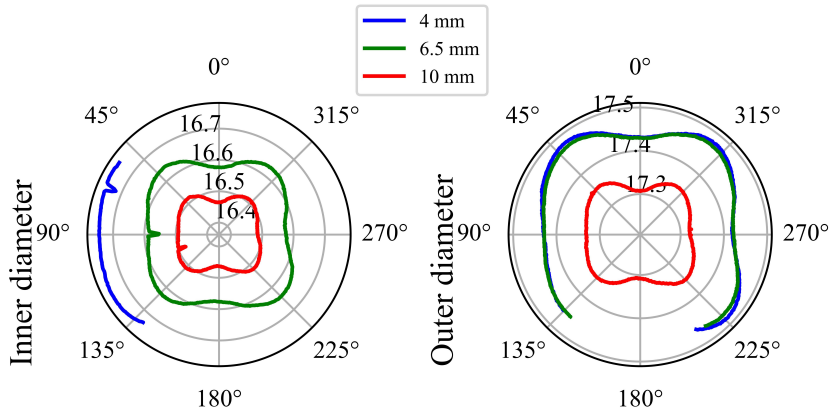


Figure 10. Deep drawing, 1.4307 blank, 45° orientation, cup 6 (missing points at 4 mm in the inner profile)

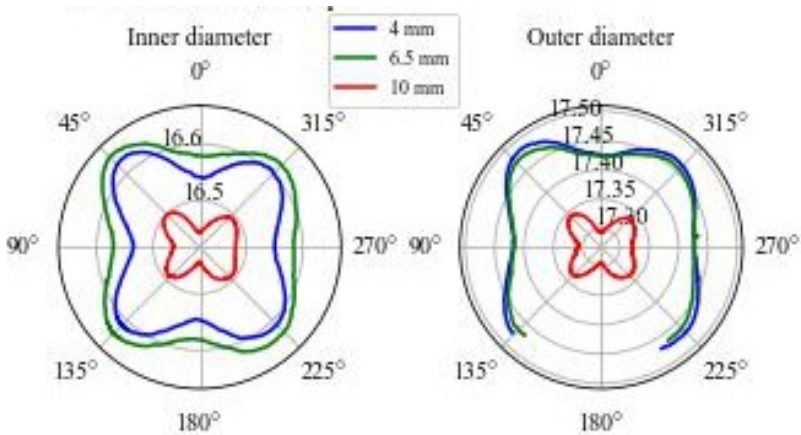


Figure 11. Deep drawing, 1.4307 blank, 90° orientation, cup 4

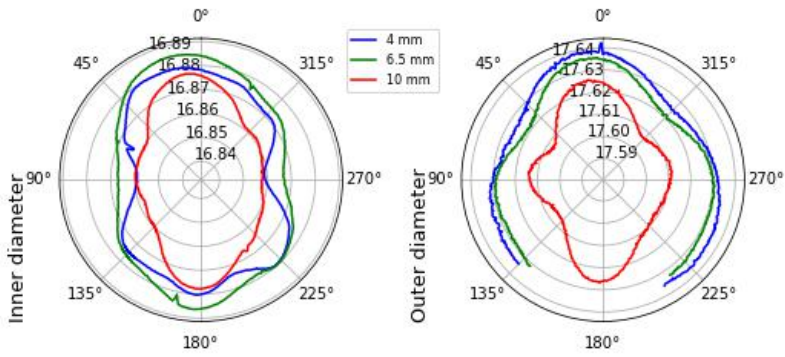


Figure 12. Ironing, 1.4404 blank, 0° orientation, cup 0

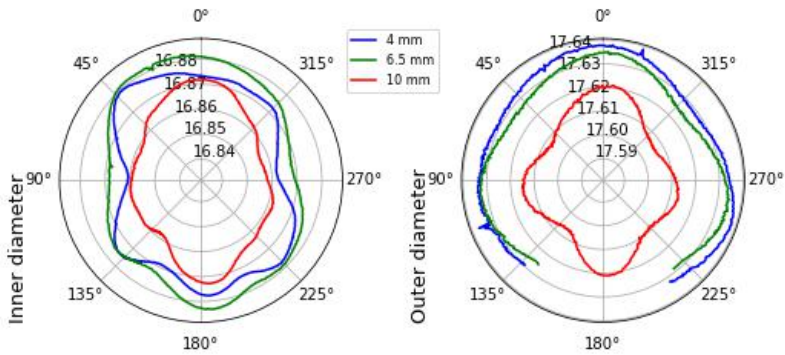


Figure 13. Ironing, 1.4404 blank, 0° orientation, cup 2

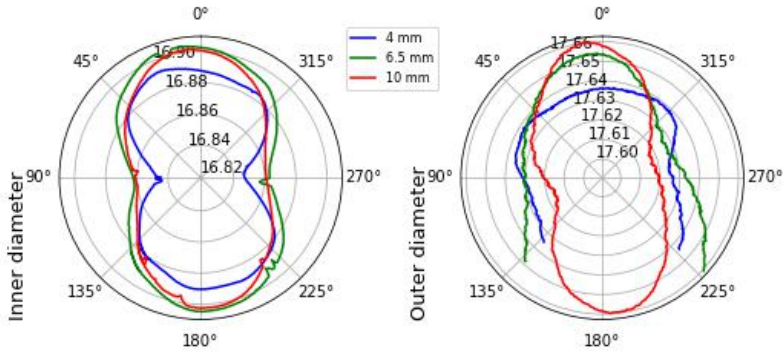


Figure 14. Ironing, 1.4404 blank, 45° orientation, cup 0

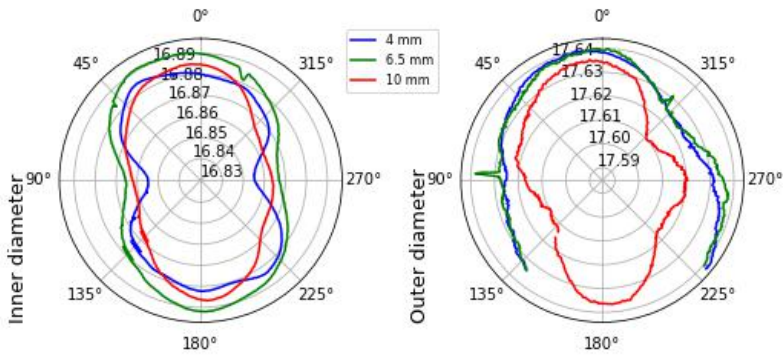


Figure 15. Ironing, 1.4404 blank, 90° orientation, cup 0

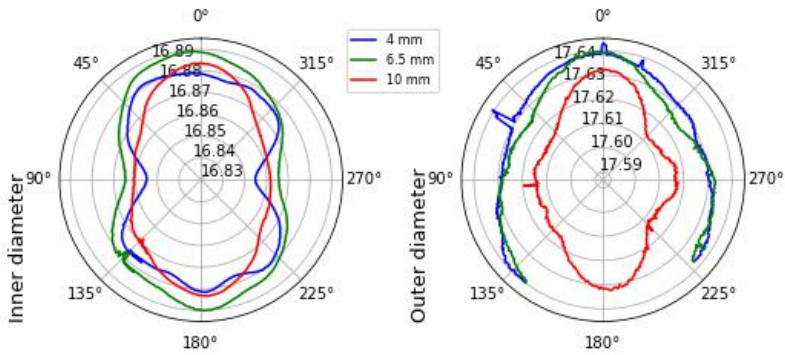


Figure 16. Ironing, 1.4404 blank, 90° orientation, cup 2

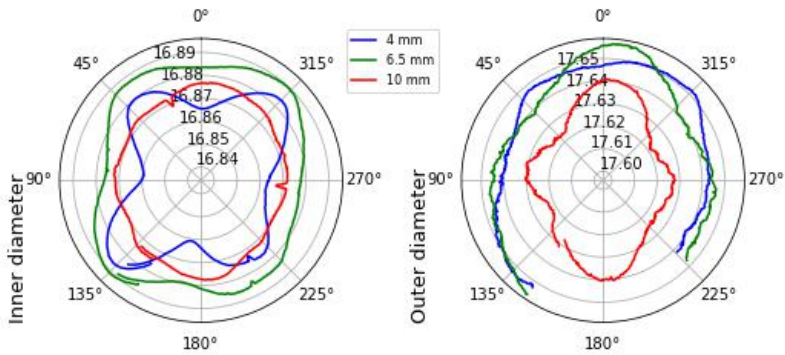


Figure 17. Ironing, 1.4307 blank, 0° orientation, cup 0

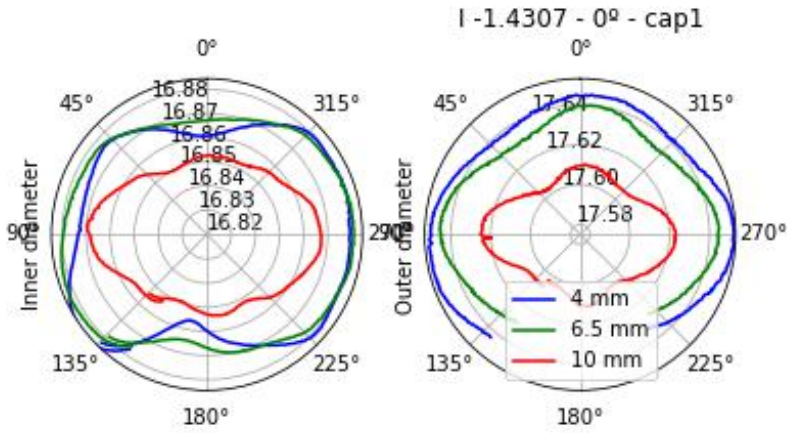


Figure 18. Ironing, 1.4307 blank, 0° orientation, cup 1

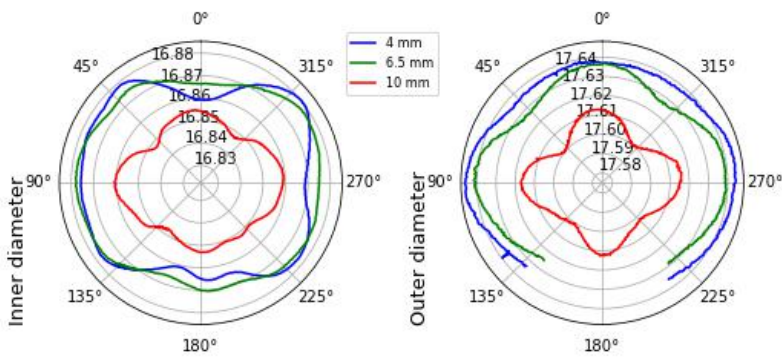


Figure 19. Ironing, 1.4307 blank, 45° orientation, cup 2

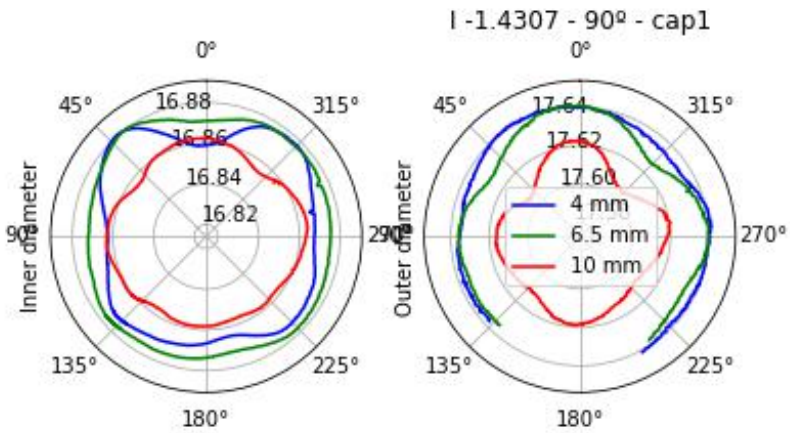


Figure 20. Ironing, 1.4307 blank, 90° orientation, cup 1

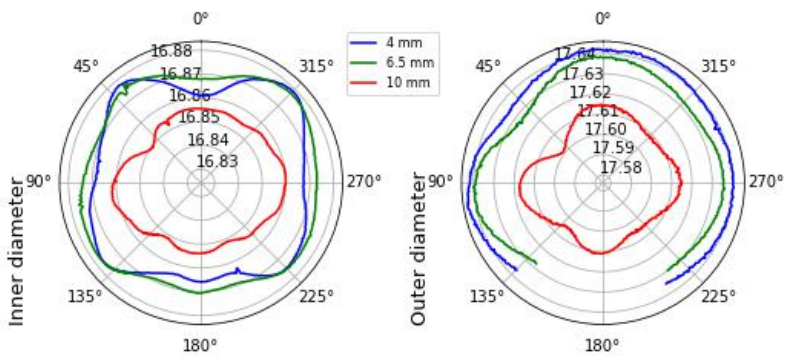



Figure 21. Ironing, 1.4307 blank, 90° orientation, cup 3


Calibration Certificates

Axial extensometer



ACCREDITED
CALIBRATION LABORATORY
CERT# 13418

Test Certificate



Epsilon
TECHNOLOGY CORP

Model: 3542-080M-050-ST
Extensometer S/N: E103065
Gage Length: 80 mm

Measuring Range: 50.0% 40 mm
Tension: -10.0% -8 mm
Compression: -10.0%

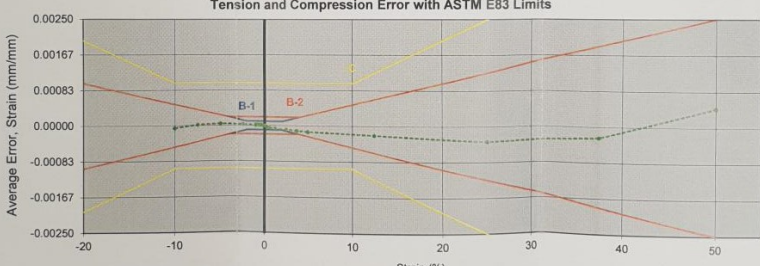
Date: 18-Feb-19

| Percent of Full Scale (%) | Actual Measuring Range | | Recorded Ext. Output | | Ext. Output | | Average Error (mV) | Average Error (%Strain) | Extensometer Class ASTM E83 |
|---------------------------|------------------------|-------------|----------------------|------------|-------------|-----------|--------------------|-------------------------|-----------------------------|
| | %Strain (%) | Displ. (mm) | RUN 1 (mV) | RUN 2 (mV) | RUN 1 (%) | RUN 2 (%) | | | |
| -100.0 | -10.000 | -8.0000 | -6.1798 | -6.1800 | -10.0052 | -10.0055 | 0.0538 | -0.0054 | A |
| -75.0 | -7.500 | -6.0000 | -4.6311 | -4.6311 | -7.4978 | -7.4978 | -0.0218 | 0.0022 | A |
| -50.0 | -5.000 | -4.0000 | -3.0855 | -3.0852 | -4.9955 | -4.9951 | -0.0473 | 0.0047 | A |
| -25.0 | -2.500 | -2.0000 | -1.5422 | -1.5419 | -2.4968 | -2.4963 | -0.0344 | 0.0034 | B-1 |
| -10.0 | -1.000 | -0.8000 | -0.6162 | -0.6165 | -0.9977 | -0.9981 | -0.0212 | 0.0021 | B-1 |
| -7.50 | -0.750 | -0.6000 | -0.4617 | -0.4621 | -0.7475 | -0.7482 | -0.0215 | 0.0022 | B-1 |
| -5.00 | -0.500 | -0.4000 | -0.3076 | -0.3075 | -0.4979 | -0.4978 | -0.0214 | 0.0021 | B-1 |
| -2.50 | -0.250 | -0.2000 | -0.1534 | -0.1538 | -0.2484 | -0.2489 | -0.0132 | 0.0013 | A |
| -1.00 | -0.100 | -0.0800 | -0.0614 | -0.0615 | -0.0995 | -0.0995 | -0.0050 | 0.0005 | A |
| -0.50 | -0.050 | -0.0400 | -0.0306 | -0.0306 | -0.0496 | -0.0495 | -0.0043 | 0.0004 | A |
| 0.00 | 0.000 | 0.0000 | 0.0000 | 0.0000 | 0.0000 | 0.0000 | 0.0000 | - | - |
| 0.50 | 0.250 | 0.2000 | 0.1525 | 0.1528 | 0.2473 | 0.2479 | -0.0048 | -0.0024 | B-1 |
| 1.00 | 0.500 | 0.4000 | 0.3051 | 0.3067 | 0.4949 | 0.4974 | -0.0077 | -0.0039 | B-1 |
| 2.50 | 1.250 | 1.0000 | 0.7658 | 0.7680 | 1.2420 | 1.2456 | -0.0123 | -0.0062 | B-1 |
| 5.00 | 2.500 | 2.0000 | 1.5341 | 1.5379 | 2.4882 | 2.4944 | -0.0174 | -0.0087 | B-1 |
| 7.50 | 3.750 | 3.0000 | 2.3026 | 2.3073 | 3.7347 | 3.7424 | -0.0230 | -0.0115 | B-1 |
| 10.0 | 5.000 | 4.0000 | 3.0716 | 3.0770 | 4.9821 | 4.9908 | -0.0272 | -0.0136 | B-1 |
| 25.0 | 12.500 | 10.0000 | 7.6914 | 7.6981 | 12.4751 | 12.4827 | -0.0422 | -0.0211 | B-1 |
| 50.0 | 25.000 | 20.0000 | 15.3860 | 15.3979 | 24.9553 | 24.9746 | -0.0700 | -0.0350 | B-1 |
| 75.0 | 37.500 | 30.0000 | 23.0954 | 23.1140 | 37.4597 | 37.4899 | -0.0504 | -0.0252 | A |
| 100.0 | 50.000 | 40.0000 | 30.8431 | 30.8658 | 50.0261 | 50.0630 | 0.0891 | 0.0445 | A |


| Excitation Voltage: 5.0000 VDC | Gage Length Error: 0.0250 % GL | Temperature: 72.50 °F | | | | | | | | | | | | | | | | | | | | | | | | | | | | | | | |
|--|---------------------------------------|------------------------------|-----------------------|--------|---------------------------|--------|----------------------------|--------|-----------------------------|------|------------------------|--------|---------------------|-----|--|----------|-----|-------|----------------|---|-----|----------------|---|-------|------------|---|-------|------------|---|-------|--------|---|--|
| <table border="1" style="width: 100%; border-collapse: collapse;"> <tr><th>Tension:</th><th>Comp.:</th></tr> <tr><td>Linearity, %FS: 0.089</td><td>-0.054</td></tr> <tr><td>Best fit span, mV: 30.827</td><td>-6.177</td></tr> <tr><td>Best fit span, mV/V: 3.083</td><td>-0.618</td></tr> <tr><td>Best fit slope, mV/mm: 0.77</td><td>0.77</td></tr> <tr><td>Hysteresis, %FS: 0.055</td><td>-0.083</td></tr> <tr><td>ASTM E83 Class: B-1</td><td>B-1</td></tr> </table> | Tension: | Comp.: | Linearity, %FS: 0.089 | -0.054 | Best fit span, mV: 30.827 | -6.177 | Best fit span, mV/V: 3.083 | -0.618 | Best fit slope, mV/mm: 0.77 | 0.77 | Hysteresis, %FS: 0.055 | -0.083 | ASTM E83 Class: B-1 | B-1 | <table border="1" style="width: 100%; border-collapse: collapse;"> <tr><th>Function</th><th>Pin</th><th>Color</th></tr> <tr><td>Excitation (+)</td><td>1</td><td>RED</td></tr> <tr><td>Excitation (-)</td><td>2</td><td>BLACK</td></tr> <tr><td>Output (+)</td><td>3</td><td>GREEN</td></tr> <tr><td>Output (-)</td><td>4</td><td>WHITE</td></tr> <tr><td>Shield</td><td>5</td><td></td></tr> </table> <p>AMP CPC Connector with Mate and Bare Leads</p> | Function | Pin | Color | Excitation (+) | 1 | RED | Excitation (-) | 2 | BLACK | Output (+) | 3 | GREEN | Output (-) | 4 | WHITE | Shield | 5 | |
| Tension: | Comp.: | | | | | | | | | | | | | | | | | | | | | | | | | | | | | | | | |
| Linearity, %FS: 0.089 | -0.054 | | | | | | | | | | | | | | | | | | | | | | | | | | | | | | | | |
| Best fit span, mV: 30.827 | -6.177 | | | | | | | | | | | | | | | | | | | | | | | | | | | | | | | | |
| Best fit span, mV/V: 3.083 | -0.618 | | | | | | | | | | | | | | | | | | | | | | | | | | | | | | | | |
| Best fit slope, mV/mm: 0.77 | 0.77 | | | | | | | | | | | | | | | | | | | | | | | | | | | | | | | | |
| Hysteresis, %FS: 0.055 | -0.083 | | | | | | | | | | | | | | | | | | | | | | | | | | | | | | | | |
| ASTM E83 Class: B-1 | B-1 | | | | | | | | | | | | | | | | | | | | | | | | | | | | | | | | |
| Function | Pin | Color | | | | | | | | | | | | | | | | | | | | | | | | | | | | | | | |
| Excitation (+) | 1 | RED | | | | | | | | | | | | | | | | | | | | | | | | | | | | | | | |
| Excitation (-) | 2 | BLACK | | | | | | | | | | | | | | | | | | | | | | | | | | | | | | | |
| Output (+) | 3 | GREEN | | | | | | | | | | | | | | | | | | | | | | | | | | | | | | | |
| Output (-) | 4 | WHITE | | | | | | | | | | | | | | | | | | | | | | | | | | | | | | | |
| Shield | 5 | | | | | | | | | | | | | | | | | | | | | | | | | | | | | | | | |


| | |
|---|---|
| Shunt Calibration Data: (With Epsilon Shunt inserted into Shunt Socket) | Shunt System: Epsilon Shunt Calibration System |
| Shunted Reading: 2.148 mV/V | Shunted Reading: 34.841 % Strain |

Tension and Compression Error with ASTM E83 Limits



| | |
|---------------------------------------|---------------------|
| Meter: Keithley 2100 | S/N: 1149144 |
| Calibrator: 3590AVHR (Epsilon) | S/N: A9007 |

Calibrated By: 

Verified By: 


Date: 18-Feb-19

Date: 19-Feb-19

Epsilon Technology
3975 S. Hwy. 89, Jackson, WY 83001
Phone: (307) 733-8360, Website: www.epsilontech.com


Page 1 of 2

Transverse extensometer



ACCREDITED
CALIBRATION LABORATORY
CERT#013481

Test Certificate



Epsilon
TECHNOLOGY CORP

| | | | | |
|---|-------------|--|--|-----------------|
| Model: 3575-500M-ST Extensometer S/N: E103364 Specimen Size: 0 to 25 mm | | Measuring Range: Tension (Inward) -5,000 mm Compression (Outward) 5,000 mm | | Date: 11-Apr-19 |
| | Output (mV) | | | |
| Travel (mm) | Run #1 | Run #2 | | |
| 5.000 | 28.110 | 28.113 | | |
| 4.000 | 22.463 | 22.465 | | |
| 3.000 | 16.826 | 16.828 | | |
| 2.000 | 11.205 | 11.205 | | |
| 1.000 | 5.594 | 5.594 | | |
| 0.000 | 0.000 | 0.000 | | |
| -1.000 | -5.583 | -5.584 | | |
| -2.000 | -11.153 | -11.153 | | |
| -3.000 | -16.709 | -16.711 | | |
| -4.000 | -22.255 | -22.256 | | |
| -5.000 | -27.785 | -27.786 | | |

Linearity, %FS: Tension: -0.107 Comp.: 0.106

Best fit span, mV: Tension: -27.815 Comp.: 28.082

Best fit span mV/V: Tension: -2.782 Comp.: 2.808

Best fit slope mV/mm: Tension: 5.563 Comp.: 5.616

Hysteresis %FS: Tension: 0.036 Comp.: 0.049

Intercept, mV: Tension: 0.000 Comp.: 0.313

Zero Output, mV: Tension: 0.313 Comp.: 0.000

Excitation Voltage: 10.000 VDC

Temperature: 71.6 °F 22.0 °C

| Wiring Config.: Function | Pin | Color |
|--------------------------|-----|-------|
| Excitation (+) | 1 | RED |
| Excitation (-) | 2 | BLACK |
| Output (+) | 3 | GREEN |
| Output (-) | 4 | WHITE |
| Shield | 5 | |

Shunt Calibration Data:

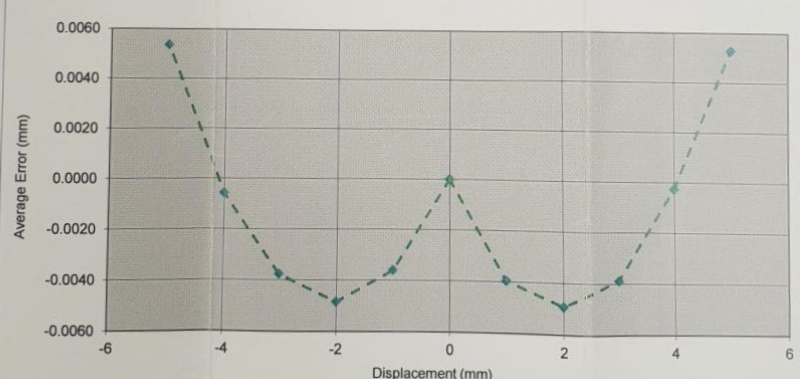
Shunt Resistor: Internal Epsilon Shunt

Shunted Reading: -2.151 mV/V

Shunted Reading: -3.866 mm

With Shunt Plugged In

AMP CPC Connector with Male and Female Leads



The graph plots Average Error (mm) on the y-axis (ranging from -0.0060 to 0.0060) against Displacement (mm) on the x-axis (ranging from -6 to 6). The data points, connected by a dashed line, show a parabolic trend with a minimum error of approximately -0.0050 mm at 0 mm displacement and maximum errors of approximately 0.0050 mm at -5 mm and 5 mm displacement.

Meter: Keithley 2100

Calibrator: 3590AVHR (Epsilon)

S/N: 1149144

S/N: A9007

Calibrated By: [Signature]

Verified By: [Signature]

Date: 11-Apr-19

Date: 12-Apr-19

Epsilon Technology
 3975 S. Hwy. 89, Jackson, WY 83001, USA
 Phone: (307) 733-8360, Website: www.epsilontech.com

Page 1 of 2

Demonstrations

Equivalent strain in plane stress

In plane stress ($\sigma_z = 0$, being σ_z the stress in the thickness direction of the flange), when R is the same in all directions, the equivalent strain is defined as:

$$\epsilon_{\text{eq}}(R, \epsilon_l, \epsilon_w, \epsilon_t) = \frac{1+R}{\sqrt{1+2R}} \cdot \sqrt{\epsilon_l^2 + \frac{2R}{1+R} \epsilon_l \epsilon_w + \epsilon_w^2} \quad (1)$$

where R is defined as

$$R = \frac{\epsilon_w}{\epsilon_t} \rightarrow \epsilon_t = \frac{\epsilon_w}{R} \quad (2)$$

Assuming volume conservation:

$$\epsilon_l + \epsilon_w + \epsilon_t = 0 \quad (3)$$

Inserting (2) in (3)

$$\begin{aligned} \epsilon_l + \left(1 + \frac{1}{R}\right) \cdot \epsilon_w &= 0 \rightarrow \\ \epsilon_w &= -\frac{\epsilon_l}{1 + \frac{1}{R}} = -\frac{R\epsilon_l}{1+R} \end{aligned} \quad (4)$$

Inserting (4) in (1):

$$\begin{aligned}
 \epsilon_{\text{eq}} &= \frac{1+R}{\sqrt{1+2R}} \cdot \sqrt{\epsilon_l^2 + \frac{2R}{1+R}\epsilon_l \cdot -\frac{R\epsilon_l}{1+R} + \left(-\frac{R\epsilon_l}{1+R}\right)^2} \\
 &= \frac{1+R}{\sqrt{1+2R}} \cdot \sqrt{1 - \frac{R^2}{(1+R)^2} \cdot \frac{1+R}{\sqrt{1+2R}} \cdot \epsilon_l} \\
 &= \epsilon_l \cdot \sqrt{\frac{(1+R)^2}{1+2R} \cdot \frac{(1+R)^2 - R^2}{(1+R)^2}} \\
 &= \epsilon_l \cdot \sqrt{\frac{(1+R)^2 - R^2}{1+2R}} \\
 &= \epsilon_l \cdot \sqrt{\frac{1+2R+R^2-R^2}{1+2R}} \\
 &= \epsilon_l
 \end{aligned}$$

↓

$$\boxed{\epsilon_{\text{eq}} = \epsilon_l}$$

(5)

Sustainable Development Goals

This project suits the following European Union Sustainable Development Goals established in 2015 by the United Nations General Assembly intended to be achieved by 2030.

| Sustainable Development Goal | High | Medium | Low | Non-Applicable |
|--|------|--------|-----|----------------|
| 1. No poverty | | | | x |
| 2. Zero hunger | | | | x |
| 3. Good health and well-being | | | | x |
| 4. Quality Education | | | | x |
| 5. Gender Equality | | | | x |
| 6. Clean water and sanitation | | | | x |
| 7. Affordable and clean energy | | | | x |
| 8. Decent work and economic growth | | | | x |
| 9. Industry, innovation, and infrastructure | x | | | |
| 10. Reduce inequalities | | | | x |
| 11. Sustainable cities and communities | | | | x |
| 12. Responsible consumption and production | x | | | |
| 13. Climate action | | | | x |
| 14. Life below water | | | | x |
| 15. Life on land | | | x | |
| 16. Peace, justice and strong institutions | | | | x |
| 17. Partnerships for the goals | | | | x |

Table 1. European Union Sustainable Development Goals